

THE STELLAR WINDS ATLAS I: CURRENT UNCERTAINTIES IN MASS-LOSS RATES

AMEDEO ROMAGNOLO[✉]

Universität Heidelberg, Zentrum für Astronomie (ZAH), Institut für Theoretische Astrophysik, Albert Ueberle Str. 2, 69120, Heidelberg, Germany
 Dipartimento di Fisica e Astronomia Galileo Galilei, Università di Padova, Vico dell’Osservatorio 3, I-35122 Padova, Italy
 Department of Astronomy and Astrophysics, University of California, San Diego, La Jolla, CA 92093, USA and
 Nicolaus Copernicus Astronomical Center, Polish Academy of Sciences, ul. Bartycka 18, 00-716 Warsaw, Poland

FLOOR S. BROEKGAARDEN[✉]

Department of Astronomy and Astrophysics, University of California, San Diego, La Jolla, CA 92093, USA

KONSTANTINOS ANTONIADIS

IAASARS, National Observatory of Athens, 15236 Penteli, Greece and
 National and Kapodistrian University of Athens, 15784 Athens, Greece

ALEX C. GORMAZ-MATAMALA[✉]

Astronomický ústav, Akademie věd České republiky, Fričova 298, 251 65 Ondřejov, Czech Republic
Version January 6, 2026

Abstract

Stellar winds are a major source of uncertainty in understanding the life and deaths of massive stars. Across studies in the field, prescriptions for stellar winds differ substantially in both their physical assumptions and implementation, making them a dominant contributor to model-to-model variation. In this work, we present a systematic analysis of the physical assumptions underlying commonly adopted wind prescriptions for optically thin and optically thick winds of hot stars, as well as the winds of cool supergiants. Our analysis reveals substantial discrepancies across all regimes: predicted mass-loss rates for optically thin winds differ by more than an order of magnitude, while rates for cool supergiants vary by several orders of magnitude, with even wider uncertainties arising in extrapolation regimes beyond the Humphreys-Davidson limit. These disparities introduce significant ambiguity into the predicted formation of Wolf-Rayet (WR) stars, a problem further compounded by the inconsistent application of transition criteria. A central issue is the "cool Wolf-Rayet problem", a temperature regime where the classical electron-scattering Eddington factor (Γ_e) loses physical consistency. Because this factor is widely used to determine WR mass-loss rates, its failure forces models to rely on uncertain extrapolations and ad-hoc corrections. We conclude that the dominant stellar wind uncertainties arise from a mismatch between the physical assumptions in stellar wind models and the structure of the stars to which they are applied. Our framework clarifies the origins of current theoretical discrepancies and identifies the key physical bottlenecks that must be addressed to improve mass-loss modeling for massive stars.

Subject headings: Stars: evolution, Stars: massive, Stars: mass-loss, Stars: supergiants, Stars: winds, outflows

1. INTRODUCTION

The evolution of massive stars with zero-age main sequence (ZAMS) masses $M_{\text{ZAMS}} \gtrsim 20 M_{\odot}$ is fundamentally shaped by mass loss through powerful stellar winds (Meynet et al. 1994; Eggenberger et al. 2021; Garcia et al. 2025). These winds regulate the internal structure of massive stars—including their radial expansion (e.g., Belczynski et al. 2022; Romagnolo et al. 2023; Gilkis et al. 2025)—determine their final mass at core-collapse or pair-instability, and impact their galactic environments through mechanical feedback and chemical enrichment (Maeder 1983; Dray et al. 2003; Dray & Tout 2003; Limongi & Chieffi 2006; Sander & Vink 2020; Farmer et al. 2021; Martinet et al. 2022; Higgins et al. 2023; Josiek et al. 2024). Consequently, stellar evolution models rely on wind

prescriptions or “recipes” to determine mass-loss rates (\dot{M}), yet the formulation and calibration of these recipes remain major challenges in stellar astrophysics.

For hot, massive stars, stellar winds are line-driven (Lucy & Solomon 1970), with mass-loss rates that depend sensitively on luminosity and metallicity (Abbott 1982; Pauldrach et al. 1986; Kudritzki et al. 1987). These winds are broadly categorized as either *optically thin* or *optically thick*. OB-type stars exhibit optically thin winds, in which momentum is transferred to the stellar material primarily through single-line scattering of photons from the photosphere with ions. As these stars evolve, their winds can transition to an optically thick regime, producing denser outflows and substantially higher mass-loss rates (from roughly 10^{-9} – $10^{-4.5}$ to 10^{-5} – $10^{-3} M_{\odot} \text{ yr}^{-1}$; Kudritzki & Puls 2000; Gormaz-Matamala et al. 2024; Romagnolo et al. 2024) characteristic of Wolf-Rayet (WR) stars. The

transition to thick winds (i.e. WR) is still a subject of debate. Canonically, most 1D evolutionary models defined it as the evolutionary point at which the stellar surface would deplete its hydrogen abundance (X_{surf}) below a specific threshold (e.g., [Ekström et al. 2008](#); [Glebbeek et al. 2009](#)). More recently, such transition to thick winds has been updated to be a function of either the electron-scattering Eddington factor Γ_e ([Bestenlehner 2020](#)) or the wind efficiency η ([Sabahait et al. 2022](#)), which is directly correlated with the optical depth of the stellar photosphere (see for more details Sections 3.2.1, 3.2.2, and 3.2.3).

As massive stars between roughly 8 and $30 M_\odot$ ([Meynet & Maeder 2003](#)) cool and expand into the yellow supergiant (YSG) and red supergiant (RSG) phases, the driving mechanism of their winds shifts away from line-driven, but the dominant physical process dominating mass loss in these cool supergiants remains poorly understood. A cool supergiant wind interpretation involves dust-driven mass loss ([Reimers 1975](#)), enabled by dust formation at effective temperatures $T_{\text{eff}} \lesssim 1.5 \text{ kK}$ ([Field 1974](#); [Höfner & Olofsson 2018](#)). If dust can condense in the extended stellar atmosphere, its sufficiently high opacity would allow radiation pressure to efficiently expel material ([Hoyle & Wickramasinghe 1962](#)). However, a major challenge is lifting gas high enough for dust condensation to occur. Proposed mechanisms, such as strong near-surface convection and radial pulsations ([Yoon & Cantiello 2010](#))—similar to those in asymptotic giant branch (AGB) stars ([Höfner et al. 2003](#); [Neilson & Lester 2008](#))—have been shown to be insufficient for cool supergiants, which are hotter and exhibit smaller pulsation amplitudes than their AGB counterparts ([Arroyo-Torres et al. 2015](#)).

Alternative ideas have emerged in the field. Atmospheric turbulent pressure may be the primary driver of the outflow, with dust forming as a consequence rather than a cause ([Kee et al. 2021](#)), reframing dust as a byproduct of the wind, rather than its primary cause, though it may subsequently enhance the outflow due to its high opacity. More recently, [Fuller & Tsuna \(2024\)](#) proposed a “boil-off” mechanism in which shocks from vigorous near-surface convection inject momentum into the atmosphere, producing mass-loss rates highly sensitive to the ratio of convective to escape velocities. These competing physical models produce large uncertainties in existing mass-loss prescriptions, especially for YSGs, where observational constraints are sparse, and for the most luminous supergiants approaching the Humphrey-Davidson (HD) limit ([Humphreys & Davidson 1979, 1994](#)), where prescriptions require extrapolation far beyond empirically calibrated regimes.

Given these theoretical foundations, constructing universal, physically consistent mass-loss prescriptions has proved challenging. Discrepancies between prescriptions grow particularly large for stars near the Eddington limit, in late evolutionary stages, or during phenomena not captured self-consistently in 1D stellar models—such as luminous blue variable (LBV) outbursts past the HD limit. The choice of a specific wind prescription is therefore far more than a technical input: it propagates through stellar models and can yield dramatically different evolutionary outcomes. This is apparent in predictions of surface abundances (e.g. [Martinet et al. 2022](#)), stellar rotation rates (e.g. [Limongi & Chieffi 2018](#)), and final fates (e.g. [Renzo & Smith 2024](#)). At solar metallicity (Z_\odot)—an environment with rich observational constraints ([Martins et al. 2005](#); [Crowther et al. 2010](#); [Clark et al. 2012](#))—recent studies have reported a wide range of final black hole (BH) masses owing to differences in adopted mixing and wind schemes

(e.g. [Bavera et al. 2023](#); [Gilkis & Mazeh 2024](#); [Romagnolo et al. 2024](#); [Costa et al. 2025](#); [Hirschi et al. 2025](#); [Ugolini et al. 2025](#)). This divergence is driving renewed debate about the reliability of existing wind prescriptions and highlights the urgent need for systematic comparison.

In this work, we present a pedagogical overview of several widely-used stellar wind prescriptions for isolated massive stars, situating our analysis within ongoing debates to understand and quantify the dominant sources of uncertainty in wind modeling. Our methods are described in Section 2. Section 3 examines line-driven winds and the assumptions behind recipes for both optically thin and optically thick regimes, with particular attention to the uncertain transition between them. Section 4 focuses on cool supergiant winds, comparing canonical and recent prescriptions and discussing challenges associated with the YSG phase and extrapolations near the HD limit. Finally, Section 5 gives an overview of other sources of uncertainty that are not covered by the other sections. Through this systematic comparison, we aim to provide a unified framework for interpreting theoretical discrepancies and identifying key bottlenecks in stellar-wind modeling.

2. METHOD

Our approach is a direct, side-by-side comparison of commonly-used stellar wind recipes, evaluated independently of the complexities inherent to full stellar evolution simulations. A list of stellar-wind prescriptions is provided in Table 1. We compute mass-loss rates directly from the published analytical formulae, fitting functions, or tabulated data associated with each wind recipe. To maintain a uniform and systematic comparison, we restrict our analysis to closed-form, analytical mass-loss prescriptions parameterized primarily by global stellar surface quantities (L , M , T_{eff} , Z). We explicitly exclude hydrodynamically motivated models that require iterative solutions to the momentum equation or depend on detailed near-surface velocity fields (e.g., [Kee et al. 2021](#); [Fuller & Tsuna 2024](#)). Although these models offer a more physically grounded approach of mass loss through atmospheric turbulence or convective boil-off, their implementation is strongly tied to the underlying stellar structure. Because our goal is to isolate discrepancies arising from the wind recipes themselves, independent of the underlying stellar structure model choices for treatment of convection, these turbulent-pressure-driven models are beyond the scope our wind Atlas’s direct comparison.

The prescriptions analyzed here, listed with their acronyms and sources in Table 1, are selected to represent a broad and representative sample of those wind models currently employed in massive star evolution and population synthesis studies. Our selection includes both foundational, widely-adopted recipes (e.g., [de Jager et al. 1988](#); [Nugis & Lamers 2000](#); [Vink et al. 2001](#)) and more recent recipes that incorporate updated physics or new observational constraints (e.g., [Bestenlehner 2020](#); [Gormaz-Matamala et al. 2023](#); [Antoniadis et al. 2024](#); [Pauli et al. 2025](#)). This curated set provides a comprehensive overview of the landscape of theoretical uncertainties relevant to massive-star modeling. We discuss the optically thin and thick winds models and present their comparisons in Section 3, and similarly discuss the cool supergiant wind models and present their comparisons in Section 4. A summary of recent stellar evolutionary models and their associated wind schemes is provided in Table 2.

We evaluate the mass-loss rates with the analytical formulations from each presented wind models within a set parameter

TABLE 1
OVERVIEW OF THE STELLAR-WIND PRESCRIPTIONS COMPARED IN THIS WORK.

ID	Reference
R75	Reimers (1975)
PP86	Paczynski & Proszynski (1986)
dJ88	de Jager et al. (1988)
NdJ90	Nieuwenhuijzen & de Jager (1990)
HaK98	Hamann & Koesterke (1998) ^a
H00	Hurley et al. (2000)
NL00	Nugis & Lamers (2000)
C01	Crowther (2001)
V01	Vink et al. (2001)
vL05	van Loon et al. (2005)
EV06	Eldridge & Vink (2006)
Y06	Yoon et al. (2006)
GH08	Gräfener & Hamann (2008)
Bk10	Belczynski et al. (2010)
V11	Vink et al. (2011)
LC18	Limongi & Chieffi (2018)
V17	Vink (2017)
S19	Sander et al. (2019)
Sh19	Shenar et al. (2019) ^b
B20	Bestenlehner (2020) ^c
SV20	Sander & Vink (2020)
VS21	Vink & Sander (2021)
Be23	Beasor et al. (2023)
Bj23	Björklund et al. (2023)
GM23	Gormaz-Matamala et al. (2023)
Ya23	Yang et al. (2023)
A24	Antoniadis et al. (2024) ^d
D24	Decin et al. (2024)
K24	Krtička et al. (2024)
K25	Krtička et al. (2025)
P25	Pauli et al. (2025)

^a With Vink & de Koter 2005 Z -dependence as introduced in Belczynski et al. 2010.

^b Corrected tailored fits from Shenar et al. 2020.

^c With Brands et al. 2022 Z -dependence.

^d Corrected fits from Antoniadis et al. 2025a.

space at solar metallicity, $Z_{\odot} = 0.0142$ (Asplund et al. 2009), a regime where mass loss is strong and Milky Way massive stars offer observational constraints (e.g., Martins et al. 2005; Crowther et al. 2010; Clark et al. 2012). This parameter choice provides a well-studied, uniform baseline that allows a clean comparison across recipes. When a prescription's original calibration does not span the full parameter space required for our comparison, we apply extrapolations and suggest alternative calibration options.

2.1. MESA models

To demonstrate how certain physical criteria depend on the underlying stellar structure, we compute a dedicated grid of stellar models using Modules for Experiments in Stellar Astrophysics (MESA Paxton et al. 2011, 2013, 2015, 2018, 2019; Jermyn et al. 2023), version 24.08.1.

Input Physics— We adopt the Ledoux criterion (Ledoux 1947) for convective boundaries with a mixing length parameter of $\alpha_{MLT} = 1.82$ and exponential overshooting with a parameter $f_{ov} = 0.05$. We include rotation with an initial ratio of angular velocity to critical velocity of $\Omega/\Omega_{crit} = 0.4$. Rotational mixing and associated mass-loss enhancement (Friend & Abbott 1986; Langer 1998) follow the calibration of Heger et al. (2000), while magnetic angular momentum transport is modeled via the Tayler-Spruit dynamo (Tayler 1973; Spruit 2002;

Heger et al. 2005).

2.1.1. Wind Scheme Implementations

To evaluate the model dependence of transition criteria (see Section 3.2) and explore variability across different physical assumptions (see Section 3.3), we implemented the following wind configurations:

- Standard Dutch wind scheme: We use this case to explore variability with metallicity calibrations and rotation, serving as a standard baseline due to its wide use in research papers (Glebbeek et al. 2009).
- Strong Winds Eta (SWE): We use this case to represent a strong mass-loss scenario. This configuration applies Vink et al. (2001) for thin and low- Γ_e thick winds (see more in Section 3.2.2). It applies de Jager et al. (1988) for $T_{eff} < 4$ kK, Vink et al. (2011) for high- Γ_e thick winds, and Sander & Vink (2020) for $T_{eff} > 10^2$ kK. This setup modifies the original Sabhahit et al. (2023) framework by incorporating the dynamic efficiency calculations described in Section 3.2.3.
- Weak Winds Eta (WWE): We use this case to represent a "weak" mass-loss scenario. This configuration is the same of SWE, but combines mass-loss rates from Gormaz-Matamala et al. (2023) for surface gravities $\log g > 3.0$ and Vink et al. (2001) for lower gravities.
- Slavic winds: Krtička et al. (2024) for thin winds¹ and WRs at $T_{eff} < 30$ kK, Bestenlehner (2020) ($X_{surf} \geq 10^{-7}$) or Sander & Vink (2020) ($X_{surf} < 10^{-7}$) for warm WRs, Antoniadis et al. (2024) at $T_{eff} \leq 4$ kK, de Jager et al. (1988) at $T_{eff} \leq 10$ kK, and transition to thick winds as $\eta \geq \eta_{trans}$ or $\Gamma_e \geq 0.5$ (Section 3.2.1), whatever comes first. The name comes as a reference to the Dutch winds model, and is motivated by the fact that A. Romagnolo and A. C. Gormaz-Matamala developed it between Warsaw (Poland) and Prague (Czechia), and because Krtička et al. (2024) is a Czech-lead study.
- Strong Winds Gamma (SWG) model: We use this case to represent a strong mass-loss scenario based on the Γ_e transition to thick winds (Section 3.2.1). Vink et al. (2001) for thin winds and cool WRs, Bestenlehner (2020) ($X_{surf} < 10^{-7}$) or Sander & Vink (2020) ($X_{surf} \geq 10^{-7}$) for warm WRs, de Jager et al. (1988) at $T_{eff} < 10$ kK, and $\Gamma_e \geq 0.5$ transition to thick winds.

2.1.2. Argus: automated stellar winds dictionary

Argus: an automated, Large Language Model (LLM)-driven builder for the Stellar Winds Atlas. While standard reproduction packages provide static files, Argus introduces a dynamic approach to modeling. It consists of a specialized context dictionary designed for LLMs. This file encodes the structural logic of our MESA *inlist* and *run_star_extras* files, which are able to initiate stellar evolution simulations with any of the winds prescriptions from Table 1, alongside their respective recommended parameter spaces.

By uploading this dictionary alongside our default *inlist_project* to an LLM (e.g., Claude, Gemini, ChatGPT,

¹ At $Z \lesssim 0.2Z_{\odot}$ we recommend the use of Krtička et al. (2025), since the driving elements for winds are different and mass-loss rates follow a different behavior.

TABLE 2

ATLAS OF MASSIVE-STAR EVOLUTIONARY MODELS FROM THIS WORK AND THE LITERATURE, SUMMARIZING THE WIND PRESCRIPTIONS IMPLEMENTED IN EACH FRAMEWORK.

Model	Line-driven (Section 3)			Cool supergiants (Section 4)		LBV
	Thin winds \dot{M}	Thick winds trans.	\dot{M}	Transition T_{eff}	\dot{M}	
WWE	GM23, V01	$\eta > \eta_{\text{trans}}^{\text{a}}$	V11	4 kK	dJ88	—
SWE	V01	$\eta > \eta_{\text{trans}}^{\text{a}}$	V11	4 kK	dJ88	—
Slavic winds	K24	$\eta, \Gamma_e^{\text{b}}$	B20, SV20	10 kK	dJ88, A24	—
SWG	V01	$\Gamma_e > \Gamma_{e,\text{trans}}^{\text{b}}$	B20	10 kK	dJ88	—
Costa et al. (2025)	V01, GH08, V11	$X_{\text{surf}} < 0.3$	S19 ^c	10 kK	dJ88 ^d	—
Gilkis et al. (2025)	VS21, V17	$\Gamma_e > \Gamma_{e,\text{trans}}$	GH08, Sh19, SV20	22 kK	dJ88, VS21	—
Gormaz-Matamala et al. (2025b)	GM23, V01	$X_{\text{surf}}, \Gamma_e^{\text{b}}$	B20, SV20	10 kK	dJ88, Ya23	—
Gormaz-Matamala et al. (2025a)	GM23, V01	$X_{\text{surf}}, \Gamma_e^{\text{b}}$	B20, SV20	10 kK	dJ88	—
Hirschi et al. (2025)	V01	$X_{\text{surf}} < 0.3$	NL00, EV06, GH08	$10^{3.9}$ K	dJ88	—
Keszthelyi et al. (2025)	B20	$X_{\text{surf}} < 0.4$	SV20	10 kK	dJ88, vL05	—
Romagnolo et al. (2025)	0.5×V01	$X_{\text{surf}} < 0.4$	0.5×NL00	10 kK	0.5×dJ88	—
Ugolini et al. (2025)	V01	$X_{\text{surf}} < 0.4$	NL00	12 kK	dJ88, vL05	LC18
Cheng et al. (2024)	0.8×V01	$X_{\text{surf}} < 0.4$	0.8×NL00	4 kK	D24	Original
Josiek et al. (2024)	V01 or B20	$\Gamma_e > \Gamma_{e,\text{trans}}^{\text{b}}$	NL00, EV06, GH08	10 kK	dJ88, C01	—
Romagnolo et al. (2024)	GM23, V01	$X_{\text{surf}}, \Gamma_e^{\text{b}}$	B20, SV20	10 kK	dJ88	—
Sabahit et al. (2023)	V01	$\eta > \eta_{\text{trans}}^{\text{a}}$	V11, SV20	4 kK	dJ88	—
Keszthelyi et al. (2022)	0.5×V01	$X_{\text{surf}} < 0.4$	NL00	10 kK	vL05	—
Eggenberger et al. (2021)	V01	$X_{\text{surf}} < 0.3$	NL00, EV06, GH08	$10^{3.9}$ K	dJ88	—
Agrawal et al. (2020)	V01	$L/L_{\text{edd}} > 1.1$	0.1×PP86	10 kK	dJ88	—
Klencki et al. (2020)	V01, NdJ90	$\Gamma_e > \Gamma_{e,\text{trans}}$	Y06	10 kK	dJ88	—
Dutch winds	V01	$X_{\text{surf}} < 0.4$	NL00	10 kK	dJ88	—
Population synthesis codes						
StarTrack (Belczynski et al. 2010)	V01 or NdJ90	H00	HaK98	12.5 kK	NdJ90	Original
COMPAS (Merritt et al. 2025)	VS21	$\eta > \eta_{\text{trans}}^{\text{f}}$	V11, SV20	8 kK	D24	Bk10
SeBa (Dorozsma & Toonen 2024)	V01, NdJ90	H00	SV20	8 kK	R75, NdJ90	Bk10
BINARY_C (Hendriks et al. 2023)	V01	H00	Y07	11 kK	R75	H00
COSMIC (Breivik et al. 2020)	V01	H00	HaK98	12.5 kK	NdJ90	Bk10
NBODY7/BSE (Banerjee et al. 2020)	V01	H00	HaK98	12.5 kK	NdJ90	Bk10
MOCCA (Kamlah et al. 2022)	V01	H00	HaK98	12.5 kK	NdJ90	Bk10
TRES ^g (Toonen et al. 2016)	V01, NdJ90	H00	SV20	8 kK	R75, NdJ90	Bk10
POSYDON ^g v2 (Andrews et al. 2024)	V01	$X_{\text{surf}} < 0.4$	NL00	10 kK	dJ88	Bk10
SEVN ^g (Iorio et al. 2023)	V01, GH08, V11	$X_{\text{surf}} < 0.3$	S19 ^c	10 kK	dJ88 ^d	—

^aFor decreasing Γ_e or Γ_e values lower than the one at thick winds transition, the optically thin mass loss is still applied

^bFor cool WR stars ($T_{\text{eff}} < 30$ kK), the optically thin mass loss is still applied

^cMetallicity-dependent mass loss calibration from Vink et al. (2001)

^dWith Z-dependence of Costa et al. 2021, derived with fits from Vink 2015.

^eCalculation of η , η_{trans} , and Γ_e under assuming that the star is chemically homogeneous (see Section 3.2.2).

^fCalibrations for population synthesis from Merritt et al. (2025)

^gThese codes can interpolate detailed evolutionary simulations. Here are shown only the default stellar tracks/models presented with each code

Top panel: new models from this study (see Section 2.1.1).

Middle panel: models from a selected recent literature sample. The Dutch winds are shown separately as they represent the most widely used models in the literature.

Bottom panel: population synthesis models.

DeepSeek), users can interact with the Atlas via a natural language interface. Argus allows users to generate valid, complex MESA Atlas winds configurations by simply requesting specific physical scenarios (e.g., "Configure a model using the Slavic wind scheme at LMC metallicity, but use the oldest cool supergiant winds formulation you have for red supergiants"). The dictionary contains the physical limitations of each recipe, Argus can automatically warn users if their requested parameters fall outside calibrated regimes.

3. LINE-DRIVEN WINDS

Throughout most of their lives, massive stars dominantly lose mass through line-driven winds, which can be divided into two broad regimes: optically thin and thick—depending on the dominant scattering mechanisms (Figure 1).

At the beginning of their lives, hot OB-type stars exhibit optically thin, line-driven winds (Puls et al. 2008). In this regime, the stellar radius is well-defined at an optical depth of $\tau = 2/3$, with a subsonic velocity profile just above the surface. The wind is driven by radiation from the stellar photosphere (mostly in the ultraviolet range; Lamers & Cassinelli 1999), with momentum transferred primarily through single-line scattering. This mechanism is strongly metallicity-dependent, as

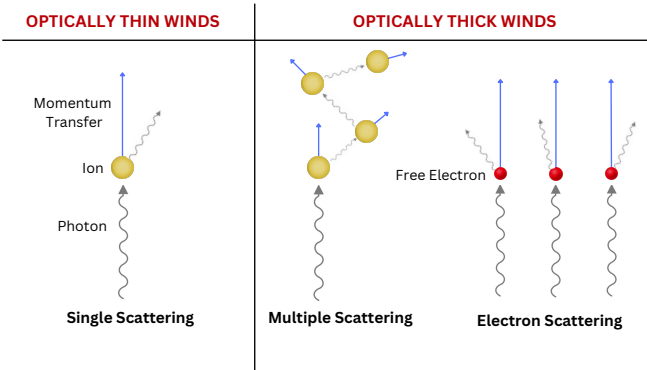


FIG. 1.— Schematic representation of the primary physical mechanisms governing optically thin and optically thick winds. All mechanisms operate to some extent in stellar atmospheres, but their relative contributions differ. In optically thin winds, single scattering processes dominate, whereas in optically thick winds, multiple scattering (i.e., deposit of more angular momentum) and free-electron (Thomson) scattering processes become the main drivers.

heavier elements provide a large number of spectral lines capable of absorbing photons. Once the sonic point recedes below the stellar surface, the stellar atmosphere transitions to an optically thick regime. The nitid separation between the photosphere and the expanded atmosphere disappears, and the wind becomes dominated by multiple scattering and free-electron scattering. These processes generate denser wind outflows with substantially higher mass-loss rates (than during the OB phase), characteristic of WR stars (Crowther 2007; Gräfener & Hamann 2008). However, the optically thick nature of these winds introduces degeneracies in standard atmospheric models that rely on prescribed wind velocity laws (Sander & Vink 2020). In particular, uncertainties in the wind stratification lead to poorly constrained radii and effective temperatures—an issue known as the “WR radius problem” (Langer et al. 1988). Hydrodynamic solutions to the equation of motion can recover self-consistent wind structures and mitigate this discrepancy.

3.1. Optically thin winds

Figure 2 shows our overview of thin winds. The most widely used prescription of mass loss in this regime comes from Vink et al. (1999, 2000, 2001), which is one of the main components of the widely-used Dutch winds model. However, this recipe predates the recognition of the role of wind clumping in OB stars, a phenomenon caused by radiative instabilities and currently widely observed in OB stars (Bouret et al. 2005; Lai et al. 2022, 2024; Verhamme et al. 2024). More recent approaches that explicitly account for wind clumping predict mass-loss rates reduced by factors 2–5 compared to older models (Bouret et al. 2005; Surlan et al. 2012, 2013; Smith 2014; Sander et al. 2017; Gormaz-Matamala et al. 2021; Pauli et al. 2025), which is also observationally justified by the fact that rotating stars were shown to not considerably spin down during main sequence (MS), suggesting therefore limited angular momentum ejection, hence weaker winds than canonically predicted (Nathaniel et al. 2025). Despite this progress, both theoretical and observational constraints on clumping (Verhamme et al. 2024; Bernini-Peron et al. 2025) and overall mass-loss rates (Backs et al. 2024) remain uncertain, and thus the classical Vink et al. (1999, 2000, 2001) prescription cannot yet be fully ruled out.

An important caveat arises for stars at an effective temperature $T_{\text{eff}} \lesssim 25$ kK. In its formulation, Vink et al. (2001)

incorporated the concept, originally proposed by Pauldrach & Puls (1990) and supported observationally by Lamers et al. (1995) and Markova & Puls (2008), of a bistability jump, where Fe III recombination increases opacity and enhances wind-driven mass loss rates by an order of magnitude. However, recent studies (Krtička et al. 2021; Björklund et al. 2023; Bernini-Peron et al. 2024; de Burgos et al. 2024; Verhamme et al. 2024; Alkousa et al. 2025) find little evidence for such a mass-loss enhancement, restricting the applicability of this recipe to a subset of hotter stars. Some recent work (Krtička et al. 2025; Bernini-Peron et al. 2023; Krtička et al. 2024) supports a weaker or metallicity-dependent bistability jump, though the onset temperature that they find varies.

3.1.1. Mass-loss rates

In Figure 2 we show our overview of the commonly-used mass-loss rates for a Z_{\odot} $35 M_{\odot}$ star with $\log(L/L_{\odot})=5.4$ across 8 kK (the YSG threshold) and 50 kK. We find that the Vink et al. (2001) and Nieuwenhuijzen & de Jager (1990) recipes yield the strongest stellar winds, with the bistability jump producing an increase of more than an order of magnitude. Evolutionary modeling shows that such strong mass loss leads to an ‘early-formed’ WNH population, whereas weaker, monotonic prescriptions such as Bestenlehner (2020) produce ‘late-formed’ WR stars that pass through a cool-supergiant phase before stripping (Josiek et al. 2024). Including the ‘second bistability jump’ proposed by Vink & Sander (2021) can further boost mass-loss rates by another order of magnitude as shown in Figure 2, though this feature remains unverified observationally (de Burgos et al. 2024; Verhamme et al. 2024). Instead, recent observations suggest that the Eddington parameter Γ_e , rather than T_{eff} , is the primary driver of enhanced mass loss (Pauli et al. 2025). Consequently, population synthesis codes adopting Nieuwenhuijzen & de Jager (1990), Vink et al. (2001), or Vink & Sander (2021) likely overestimate mass-loss rates in the optically thin winds regime, accelerating the depletion of hydrogen (H)-rich envelopes and leading to premature formation of WR stars.

3.2. Optically thick (Wolf-Rayet) winds

The mass-loss rates of optically thick winds remain highly uncertain, both theoretically and observationally, as large samples of observed WR stars are still limited (Shenar 2024). We show an overview of thick wind recipes in Figure 5. Current observations indicate at least three distinct WR populations with different mass-loss rates (WR classifications from Yusof et al. 2013; Aadland et al. 2022; Martinet et al. 2023): (i) Hydrogen (H)-rich WNL and WNH stars (Vink et al. 2011; Bestenlehner et al. 2014; Gräfener 2021); (ii) surface H(X_{surf})-poor and C/O-poor ($^{12}\text{C}+^{16}\text{O} \leq 0.03^{4}\text{He}$) WNE stars; and (iii) H-free ($X_{\text{surf}} < 10^{-7}$) and C/O rich WC and WO stars, including transitional WN/WO phases (Sander et al. 2025). Beyond the absolute mass-loss rates, a key uncertainty concerns the physical criterion that governs the onset of optically thick winds. Stellar evolution models commonly adopt a surface hydrogen threshold, X_{surf} , to trigger this transition (e.g. Ekström et al. 2008; Glebbeek et al. 2009; Eggenberger et al. 2021; Romagnolo et al. 2023; Cheng et al. 2024; Costa et al. 2025; Hirschi et al. 2025; Romagnolo et al. 2025; Ugolini et al. 2025), with values such as $X_{\text{surf}} < 0.4$ used to represent thick-wind phases in post-YSG, post-RSG, and post-LBV stars (Köhler et al. 2015). Although this criterion performs reasonably well for cool-supergiant progenitors of WR stars, it fails

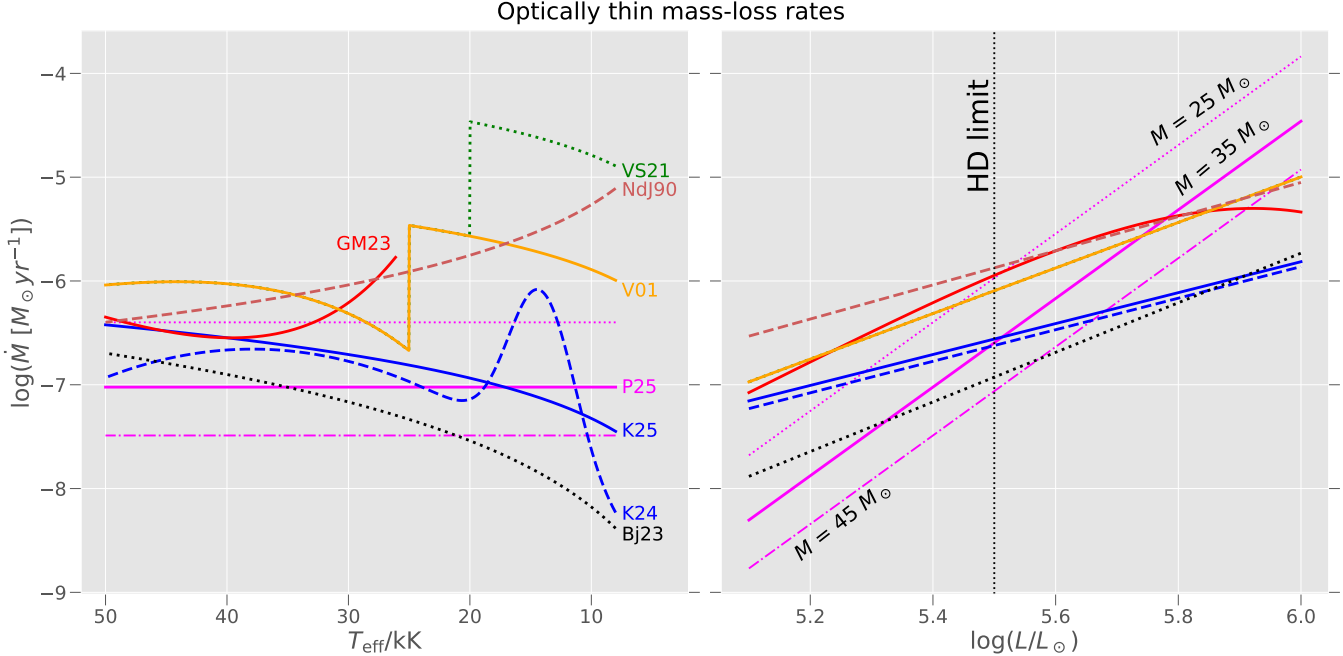


FIG. 2.— Optically thin mass-loss rates for wind recipes from the literature (acronyms listed in Table 2). Left: mass-loss rates versus effective temperature for a $35 M_{\odot}$ star and $\log(L/L_{\odot}) = 5.4$ at Z_{\odot} . Right: mass-loss rates versus luminosity for the same star at $T_{\text{eff}} = 30$ kK. The vertical dotted line marks the HD limit. The [Pauli et al. \(2025\)](#) prescription is independent of T_{eff} , and rates for this recipe are shown for masses of 25, 35, and $45 M_{\odot}$. Rates from [Gormaz-Matamala et al. \(2023\)](#) are shown only for $\log g < 3$, the limit of their stated applicability for extrapolation. The [Krtička et al. \(2025\)](#) prescription is extrapolated to solar metallicity, but only valid for $Z \lesssim 0.2 Z_{\odot}$ (see Table 3). Predictions for the mass-loss rates differ by orders of magnitude, especially for $T_{\text{eff}} < 25$ kK among models that include at least one bistability jump.

to explain (i) H-rich WN stars (e.g. [Bestenlehner et al. 2014](#); [Tehrani et al. 2019](#); [Martins & Palacios 2022](#)) and (ii) both low-mass ([Wang et al. 2017, 2018](#); [Bodensteiner et al. 2020](#); [Irrgang et al. 2020](#); [Wang et al. 2021](#); [El-Badry et al. 2022](#)) and intermediate-mass ([Drout et al. 2023](#); [Götberg et al. 2023](#)) H-poor stripped stars that do not show WR characteristics. This mismatch reflects the historical calibration of evolutionary models on classical, H-depleted late-type WR stars—the first of such objects observed—rather than on the full diversity of massive stars. In contrast, the most massive stars can display WR-like spectra, with strong emission lines and boosted mass-loss rates, from the onset of core hydrogen burning, when they are still H-rich. Thus, the physical boundary between optically thin and thick winds remains a topic of active debate. Recent hydrodynamic modeling of B hypergiants ([Bernini-Peron et al. 2025](#)) illustrates this complexity: these stars can display strong emission lines (typically interpreted as signatures of dense winds) while still possessing optically thin outflows. This decoupling between spectral appearance and (true) wind optical depth underscores the difficulty of establishing a reliable physical criterion for the emergence of true optically thick, WR-like, winds.

3.2.1. Free electron (Thomson) scattering transition

The strength of WR winds is closely linked to the Eddington factor, Γ_e , which measures the ratio of radiative to gravitational forces. As a star approaches the Eddington limit ($\Gamma_e = 1$), its mass-loss rate \dot{M} increases steeply ([Vink et al. 2011](#); [Vink & Gräfener 2012](#)). Following the classical picture of [Eddington \(1926\)](#), in which free-electron (Thomson) scattering dominates the opacity, the electron Eddington factor is

$$\Gamma_e = \frac{L\kappa_e}{4\pi c GM}, \quad (1)$$

with L is the star's luminosity, M is the star's mass, κ_e the electron-scattering opacity, c the speed of light, and G the gravitational constant. For a fully ionized plasma, this can be written (in base-10 logarithm) as

$$\log \Gamma_e = -4.813 + \log(1 + X_{\text{surf}}) + \log \frac{L}{L_{\odot}} - \log \frac{M}{M_{\odot}}. \quad (2)$$

Because of its simplicity, Γ_e is frequently used in stellar evolution codes as a switch between thin and thick wind regimes. [Bestenlehner \(2020\)](#) extended the theoretical $\dot{M} - \Gamma_e$ relation from the CAK theory introduced in [Castor et al. \(1975\)](#) toward the Eddington limit, showing that the slope of the relation changes significantly between $\Gamma_e \ll 1$ and $\Gamma_e \rightarrow 1$. Importantly, the transition point $\Gamma_{e,\text{trans}}$ is relatively robust to uncertainties in stellar atmosphere models: for stars with masses between 25 and $120 M_{\odot}$ and metallicities between $Z = 0.006$ (LMC) and $Z = 0.0142$ (solar) ([Gormaz-Matamala et al. 2022b](#))— $\Gamma_{e,\text{trans}}$ remains nearly constant at ≈ 0.48 . Consequently, many stellar evolution models adopt $\Gamma_e = 0.5$ as an approximate thin-thick wind transition for this metallicity regime ([Romagnolo et al. 2024](#); [Gormaz-Matamala et al. 2025a](#)).

Model uncertainties— This transition condition cannot be computed self-consistently in evolutionary models and must instead be calibrated using observations and stellar atmosphere simulations (see e.g. [Bestenlehner 2020](#)). At higher metallicities, free-electron scattering is not the primary driver of optically thick winds; rather, Γ_e only acts as a proxy for Fe-opacity beneath the stellar surface. Because the iron (Fe) opacity peak shifts with metallicity, $\Gamma_{e,\text{trans}}$ is not universal. [Gräfener & Hamann \(2008\)](#) showed that $\Gamma_{e,\text{trans}}$ scales inversely with Z , although their calibration differs from more recent work ([Bestenlehner 2020](#)). Thus, while $\Gamma_{e,\text{trans}} \approx 0.5$ is

appropriate for solar to LMC metallicities, it should increase towards the lower Z , reflecting the weaker Fe opacity rather than representing a fixed physical threshold.

3.2.2. Multiple scattering transition

At high metallicities, multiple scattering becomes the primary driver of optically thick winds. A self-consistent way to link this process to the onset of WR winds is based on the efficiency of its radiative momentum transfer (Gräfener et al. 2017; Gräfener 2021). Following Gräfener et al. (2017), this efficiency can be quantified with the optical depth at the sonic point τ_s and the wind efficiency parameter η ,

$$\tau_s \simeq \frac{\dot{M}v_\infty}{L/c} \left(1 + \frac{v_{\text{esc}}^2}{v_\infty^2}\right) \quad (3)$$

$$\eta \equiv \dot{M}v_\infty/(L/c) \quad (4)$$

where v_∞ is the terminal velocity and v_{esc} the escape velocity, calculated as $v_{\text{esc}} \propto \sqrt{2GM/R}$. When η exceeds the threshold

$$\eta_{\text{trans}} = 0.75 \left(1 + \frac{v_{\text{esc}}^2}{v_\infty^2}\right)^{-1} \quad (5)$$

the wind is predicted to become optically thick. The pre-factor 0.75 reflects the calibration for very massive stars from Sabhahit et al. (2023). In practice, v_∞ is approximated in the same study as

$$v_\infty = V_e^\infty \sqrt{\frac{2GM(1 - \Gamma_e)}{R}} \left(\frac{Z}{Z_\odot}\right)^{0.2} \quad (6)$$

Here, V_e^∞ represents the proportionality constant between the terminal velocity and the *effective* escape velocity ($v_{\text{esc,eff}} = v_{\text{esc}}\sqrt{1 - \Gamma_e}$), rather than the standard Newtonian escape velocity. This distinction is crucial for massive stars approaching the Eddington limit, where the $(1 - \Gamma_e)$ term significantly reduces the effective potential well. In the Sabhahit et al. (2023) model, V_e^∞ is treated as a step function: it is fixed at 2.6 for hot stars ($T_{\text{eff}} \geq 25$ kK) and drops abruptly to 1.3 at lower effective temperatures. This approximation assumes a fixed wind velocity structure that changes abruptly only at the bistability jump, lowering both v_∞ , η , and consequently the transition threshold η_{trans} in cooler regimes. However, an alternative approach is to directly adopt tabulated v_∞ profiles from detailed atmosphere models, rather than a single analytical prescription (e.g. Krtička & Kubát 2017; Björklund et al. 2021; Gormaz-Matamala et al. 2023; Krtička et al. 2025). Solving these equations, we show the existence of a natural correlation between the free-electron scattering Γ_e -based transition and the multi-scattering one:

$$\eta_{\text{trans}} = 0.75 \left(1 + \frac{1}{(V_e^\infty)^2 (Z/Z_\odot)^2} \frac{1}{1 - \Gamma_e}\right)^{-1} \quad (7)$$

Model uncertainties — The transition to thick winds is dominated by two compounding factors: the sensitivity of the wind efficiency parameter (η) to input physics and the structural assumptions used to calibrate the transition threshold (η_{trans}), the calibration of the transition value η_{trans} is based on extensive studies of the Arches and 30 Doradus clusters (Vink & Gräfener 2012; Sabhahit et al. 2022). First, η depends explicitly on the adopted mass-loss prescription (Equation 4),

representing the largest source of uncertainty due to its linear dependence on \dot{M} and the wide mass-loss variability (see Section 3.2). Stronger mass loss yields a faster increase in η , while a weaker one implies a delayed transition to the WR phase (Gormaz-Matamala et al. 2025a). Second, in the formulation of Sabhahit et al. (2023), the quantities parametrizing the transition to thick winds (Γ_e , η , and η_{trans}) are not calculated using the star's current parameters (M , L , and T_{eff}), but are instead calculated over a fixed luminosity range (10^5 to $10^8 L_\odot$) to determine a hypothetical crossing point using the properties of a chemically homogeneous star derived from the fits of Gräfener et al. (2011). This procedure appears designed to facilitate the implementation of the Vink et al. (2011) mass-loss recipe, which adopts a "multiplier" to the optically thin mass-loss rates at the onset of thick winds. Because some very massive stars are already in the WR phase near ZAMS, they lack a physical transition point from thin to thick winds in their evolutionary history; therefore, the Sabhahit et al. (2023) model effectively extrapolates a hypothetical pre-ZAMS evolution to locate a theoretical anchor point for the Vink et al. (2011) multiplier. This reliance on the chemical homogeneous mass introduces a systematic physical inconsistency. By fixing the transition calculation to chemical homogeneous mass (i.e., the maximum possible mass for a given luminosity and surface-H abundance) the model adopts a mass consistently higher than that of an evolving star. This choice artificially lowers the Eddington factor ($\Gamma_e \propto L/M$), thereby increasing the term $(1 - \Gamma_e)$. Following Equation 7, a higher $(1 - \Gamma_e)$ leads to a higher value for the transition threshold η_{trans} (see also Figure A.1 from Boco et al. 2025, in which a further analysis of the transition to thick winds is provided). Sabhahit et al. (2023) adopt this approach because very massive stars above roughly $160 M_\odot$ are thought to remain chemically homogeneous throughout the MS. However, as shown by Hirschi et al. (2025), this assumption is not universally valid and is strongly metallicity- and model-dependent: at $Z = 0.002$, even stars approaching $300 M_\odot$ may not necessarily evolve under conditions of chemical homogeneity. Although Sabhahit et al. (2023) acknowledge their framework as a "theoretical exercise" for high-redshift conditions, their reliance on a homogeneous approximation to preserve the validity of Vink et al. (2001, 2011) neglects actual surface properties. This risks introducing significant errors in WR phase duration and remnant mass, particularly for non-very massive, solar-metallicity, or low-metallicity stars where the homogeneity assumption breaks down.

3.2.3. New multi-scattering model

While the reliance on the chemically homogeneous approximation described in Section 3.2.2 limits the general applicability of the Sabhahit et al. (2023) framework, its underlying physical premise—that the transition to optically thick winds is governed by the wind efficiency η —remains robust. To preserve this physical consistency while moving beyond the calibration choices originally made to accommodate the Vink et al. (2001, 2011) models, we generalize the method to rely on the star's instantaneous surface properties. In order to calculate η and η_{trans} more self-consistently without adhering to the original restriction, we recommend the implementation of the following updates to the canonical version:

1. *Temperature-dependent velocity scaling*: The behavior of V_e^∞ as a function of effective temperature remains

a subject of active debate. While standard recipes enforce a sharp discontinuity, the work of [Crowther et al. \(2006\)](#) and recent observations of low-metallicity B-supergiants suggest a complex picture. [Bernini-Peron et al. \(2024\)](#) report a drop in V_e^∞ occurring at ~ 19 kK, significantly cooler than the canonical prediction at 25 kK. However, as noticeable in Figure 18 of [Bernini-Peron et al. \(2024\)](#), the observational data exhibit considerable scatter. While V_e^∞ is statistically larger above 20 kK than below, the distribution of individual measurements does not uniquely demand a step-function jump. A continuous, linear increase with temperature offers an equally plausible representation of the data within the errors and avoids enforcing a sharp transition at an uncertain temperature. We fit the V_e^∞ factor directly to the empirical observations of Galactic supergiants from [Crowther et al. \(2006\)](#). Figure 3 shows the linear dependency from our best-fit model $V_e^\infty = 1.59 \times 10^{-4} T_{\text{eff}} - 0.89$. For $T_{\text{eff}} \gtrsim 15$ kK, our model yields a continuous range of values for V_e^∞ that generally exceed the fixed step-function values used in [Sabahait et al. \(2023\)](#). This results in higher predicted terminal velocities, which leads to increased wind efficiency η and a higher transition threshold η_{trans} .

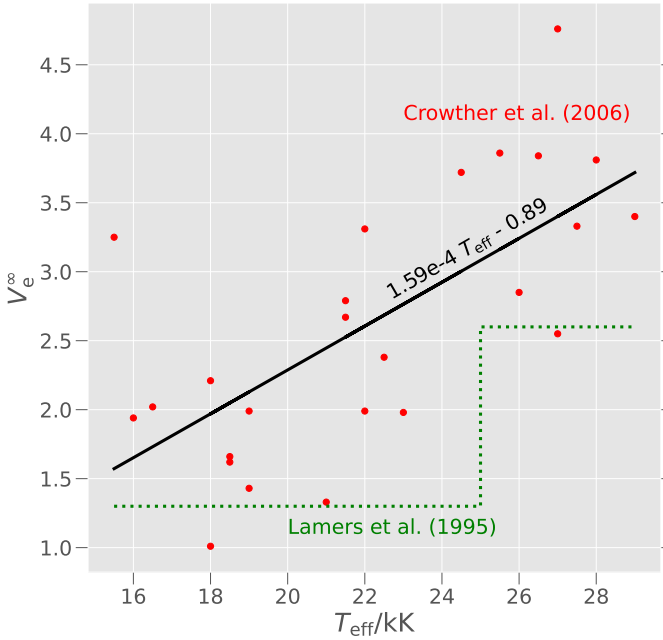


FIG. 3.— V_e^∞ observations from [Crowther et al. \(2006\)](#) as a function of effective temperature (dots). We also show our linear fit (black line) and the parametrization (green dotted line) from [Lamers et al. \(1995\)](#), used in many mass-loss models ([Vink et al. 2001, 2021; Sabahait et al. 2023](#)).

2. *Self-consistent v_∞ and v_{esc} values:* Rather than calculating v_∞ and v_{esc} from hypothetical chemically homogeneous conditions, the star’s *current* mass, luminosity, effective temperature and radius should be used in the calculations. Figure 4 illustrates the impact of this new parametrization on the WWE and SWE models, showing a strong inverse dependence on M_{ZAMS} and mass-loss.

3. *Thomson scattering Γ_e validity regime:* The transition to optically thick winds should not be allowed at

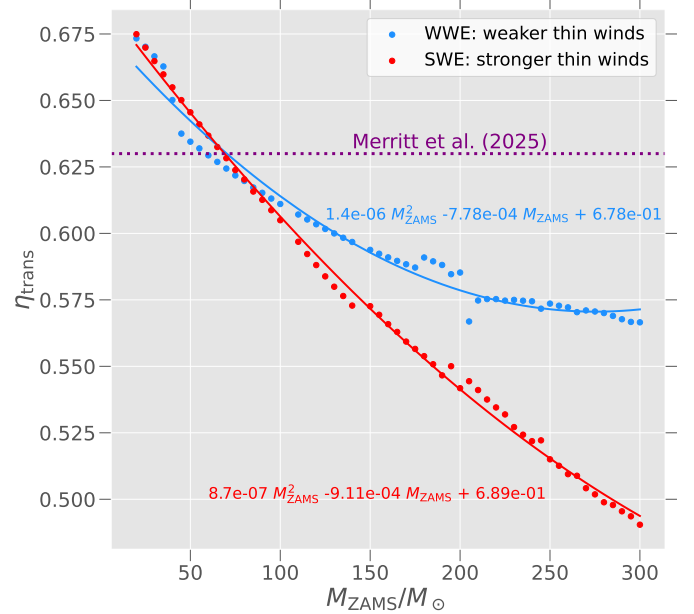


FIG. 4.— Wind efficiency transition as a function of M_{ZAMS} for solar metallicity stars at the onset of optically thick winds (dots), shown for two evolutionary models (WWE and SWE), as well as our fits for each model (lines). The value of η_{trans} is inversely proportional to M_{ZAMS} and deviates significantly from being constant as is often assumed.

$T_{\text{eff}} \leq 15$ kK, since this represents the limit of the extrapolation of the free-electron scattering physics behind the calculation of Γ_e , upon which the entire calculation of η and η_{trans} depends (see Section 3.2.5 for more details).

4. *Proximity to the Eddington limit:* Very massive stars possess surfaces that evolve close to the Eddington limit. Relying solely on the η parameter to trigger thick winds can result in an unphysical delay in the onset of the WR phase, particularly when using modern optically thin wind recipes. Because these newer prescriptions often predict lower mass-loss rates than the [Vink et al. \(2001\)](#) baseline used to calibrate η and η_{trans} in [Sabahait et al. \(2023\)](#), the resulting η values may remain artificially low. We therefore recommend supplementing the η criterion with a $\Gamma_e > \Gamma_{e,\text{trans}}$ ($\Gamma_e > 0.5$ for $Z \geq 0.008$; [Gormaz-Matamala et al. 2022b](#)) condition to ensure that the physical effects of high Eddington factors are explicitly captured.

We stress that our model for the calculation of the wind efficiency factor η is aligned with the evolving properties of stars, but was not re-calibrated with the aid of atmospheric models to fully match the transition to optically thick winds. It must be however highlighted that not even the models from [Sabahait et al. \(2023\)](#) were calibrated for the non-very massive ($M \lesssim 100 M_\odot$) regime either. Our modeling choices are aimed at providing a more model-agnostic formulation for the initiation of thick winds that could work through the whole mass spectrum regardless of the adopted recipes for thin and thick winds.

3.2.4. Mass-loss rates

Figure 5 shows the mass-loss rates predicted by several commonly used recipes for optically thick winds, evaluated for a $60 M_\odot$ star at $X_{\text{surf}} = 0.4$ (a common transition point to optically thick winds; [Ekström et al. 2008; Glebbeek et al. 2009](#))

and $T_{\text{eff}} = 30$ kK, a threshold often adopted in stellar evolution models for fully-ionized surfaces (Josiek et al. 2024; Romagnolo et al. 2024; Gormaz-Matamala et al. 2025a).

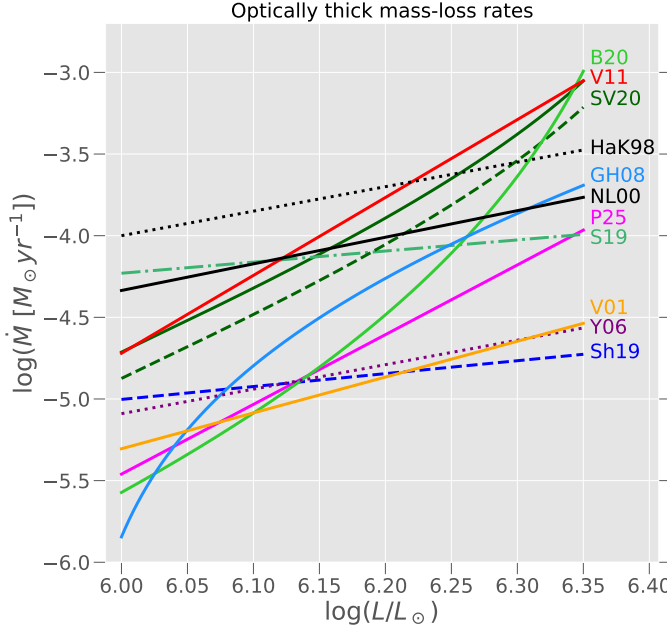


Fig. 5.— Evolution of mass-loss rates for optically thick winds as a function of luminosity for a $60 M_{\odot}$ star at Z_{\odot} , surface hydrogen fraction $X_{\text{surf}} = 0.4$, and $T_{\text{eff}} = 30$ kK, assuming $\Gamma_e \geq 0.4$. For comparison, the pre-bistability mass-loss rates from Vink et al. (2001) are shown. The dark green dashed green dark line shows the Sander et al. (2023) temperature correction applied to the Sander & Vink (2020) mass loss for $T_{\text{eff}} = 150$ kK.

We show that the mass-loss rates from Vink et al. (2001), despite representing the weaker optically thin wind regime, predict similar mass-loss rates to Yoon et al. (2006) and Shenar et al. (2019) at $\log L \gtrsim 6.3$, and higher than Gräfener & Hamann (2008); Bestenlehner (2020); Pauli et al. (2025) for $\log L \lesssim 6.05$. As highlighted by Gormaz-Matamala et al. (2022a), the low mass-loss rates from Bestenlehner (2020) are due to the fact that the star has not yet reached the transition condition to optically thick winds at $\Gamma_e \approx 0.5$, which is a requirement for their application. On the other hand, the underestimate of mass loss from Gräfener & Hamann (2008) is a well known issue in stellar evolution, which leads, for instance, the GENEC models within this regime to select at each timestep the maximum mass loss between Gräfener & Hamann (2008) and Vink et al. (2001), rather than only applying one wind recipe at a time (Eggenberger et al. 2021; Hirschi et al. 2025) (more details in Section 5).

Comparing these formulations numerically nevertheless only reveals part of the discrepancies. The fundamental reliability of these rates and the transitions between them hinges critically on the physical parameters governing the wind driving mechanism. Central to this issue is the application of the Eddington factor Γ_e , which, as we discuss next, faces significant physical contradictions when applied to cooler stars.

3.2.5. Cool WR problem: T_{eff} -dependency of Γ_e

A central theoretical bottleneck in modeling evolved massive stars is the 'cool Wolf-Rayet problem', which is a regime where the standard physical driver of mass loss loses its consistency.

The winds of massive stars are deeply dependent on the relationship between luminosity and mass, a ratio commonly represented by Γ_e . Mass-loss rates for both optically thin (e.g. Pauli et al. 2025) and optically thick winds (e.g. Bestenlehner 2020) explicitly depend on Γ_e in their formulation. Furthermore, the most widely used criteria for the transition from optically thin to optically thick winds are critically linked to this factor. For the free-electron scattering condition, it is assumed that a star develops optically thick winds when Γ_e exceeds a specific calibrated threshold. Similarly, for the multiple-scattering condition, while the transition is formally determined by the wind efficiency parameter η , in its original formulation the onset of the strong WR winds is also tied to an increasing Γ_e (Sabahit et al. 2023).

Models adopting Γ_e to stars outside a very specific, high-temperature regime introduce a significant physical inconsistency. The derivation of Γ_e is fundamentally based on the assumption that the stellar opacity is constant and dominated by a single process: Thomson scattering by free electrons in a fully ionized plasma (Eddington 1926). This "continuum opacity" assumption has a strict domain of validity. The physical prerequisite for electron scattering to be the dominant opacity source is a stellar photosphere that is almost completely ionized. This condition is only met in the hottest O-type and very early B-type stars, which have effective temperatures $T_{\text{eff}} \gtrsim 30$ kK (Bestenlehner 2020). While 30 kK represents a robust threshold for absolute Thomson dominance where H, helium (He), and CNO elements are fully ionized, a transition regime of functional validity may persist down to approximately 15 kK. In this range ($15 \text{ kK} < T_{\text{eff}} < 30 \text{ kK}$), electron scattering can still play a role in the opacity levels (Bernini-Peron et al. 2025) due to the potentially high ionization levels (see also the Saha ionization equation: Saha 1920, 1921). However, a hard physical floor exists at ≈ 15 kK. Below this temperature, the recombination of hydrogen introduces an 'opacity cliff' (Davidson 1987; Owocki 2015). As a star's photosphere cools, it is no longer fully ionized and the true Rosseland mean opacity increases, becoming orders of magnitude larger than the constant electron scattering value used to calculate the classical Γ_e . Consequently, any model that uses the classical Γ_e for stars cooler than 30 kK is not correctly estimating the true radiative force acting on the stellar material. This physical mismatch is the root of the "cool WR problem" and represents a fundamental flaw in several current mass-loss models.

The necessity of treating ionization rigorously is reinforced by X-ray observations of massive binaries. Lai et al. (2024) demonstrate that neutral wind models fail to reproduce key observational features in the color-color diagrams of Cyg X-1, explicitly requiring a partially ionized absorbing medium. This empirical evidence shows that assuming constant ionization states (like fully ionized Thomson scattering) is insufficient even for O-supergiants, let alone the cooler WR regimes discussed here.

Mass loss— At present, no dedicated mass-loss recipe exists for cool WR stars. Recent modelling of late-type WNh stars from Lefever et al. (2025) directly confronts this cool WR problem and illustrates why simple solutions are inadequate. Their work reveals that, far from a smooth extrapolation, the mass loss in this regime is complex and highly sensitive to effective temperature and metallicity. They confirm that applying prescriptions based on the classical Γ_e is flawed, not just because the opacity source is wrong (it is

highly dependent on Fe opacity gradients), but because the underlying physics leads to non-monotonic and even discontinuous behavior. This forces current evolutionary codes to employ ad-hoc workarounds. Some models revert to optically thin wind recipes for cool WR stars, even when the classical Γ_e exceeds the transition threshold (e.g. Romagnolo et al. 2024; Gormaz-Matamala et al. 2025a). Others, such as the canonical Dutch winds or models using either Gräfener & Hamann (2008) or Sabhahit et al. (2023), continue to apply strong, optically thick winds. While applying strong winds to these objects may better align with observational constraints like the HD limit (Boco et al. 2025), it is important to recognize that the theoretical justification based on the classical Γ_e is physically unsound in this temperature regime, with recent studies suggesting weaker mass loss rates (Bernini-Peron et al. 2025; Lefever et al. 2025).

Transition to thick winds— The reliance on an inconsistent physical parameter is particularly problematic for the transition criteria themselves. Both the free-electron scattering and the Sabhahit et al. (2023) multiple-scattering transition models have limitations: they check for the initiation of optically thick and/or strong WR winds as a function of the classical Γ_e , even when the star cools below 30 kK. This methodology weakens the robustness of both prescriptions. It forces the models to rely on uncertain extrapolations rather than on additional recalibrations that attempt to empirically account for the missing physics of atomic opacities. A truly predictive model for the onset of optically thick winds must incorporate a more sophisticated treatment of opacity that is valid across the full range of temperatures encountered by evolving massive stars.

3.3. Variability with Z_\odot calibrations

Wind formulations usually scale mass loss with metallicity as $\dot{M} \propto (Z/Z_\odot)^\alpha$, with α a set calibration factor and Z_\odot representing solar metallicity. Since solar metallicity does not have an universally recognized value (0.019: Anders & Grevesse 1989; 0.017: Grevesse et al. 1996; 0.0142: Asplund et al. 2009), the choice of the Z_\odot scaling factor can vary across different studies. For instance, Z_\odot was set to 0.019 in the Vink et al. (2001) original fits and to 0.0142 in Krtička et al. (2024), while for Pauli et al. (2025) the metallicity-dependency was not calibrated as a function of Z_\odot , but only as a function of the Fe abundance. All these calibrations are meant to represent the strength of the Fe lines in winds, but when different formulations are combined within stellar models to simulate different evolutionary phases of a given star (e.g. thin and thick winds), the Z_\odot scaling factor may have different calibrations for each adopted mass-loss formula. Under these conditions, common modeling choices are to either adopt the original Z_\odot values from each mass-loss prescription (as is the case for e.g., Boco et al. 2025; Costa et al. 2025; Romagnolo et al. 2025), or to merge all the different metallicity dependencies under one single Z_\odot value (e.g., GENEC and POSYDON papers, like Eggenberger et al. 2021; Bavera et al. 2023; Kruckow et al. 2024; Gormaz-Matamala et al. 2025a; Hirschi et al. 2025).

While adhering to original calibrations preserves the specific original fits, standardizing Z_\odot facilitates rigorous comparisons across mass-loss rates and offers better physical self-consistency by aligning the wind-driving Fe-group opacities with the modeled metal distribution governing stellar interiors via opacity tables. One choice is more consistent with the original wind studies while the other ensures greater physical self-consistency within evolutionary codes. Ultimately,

both approaches are not universally valid and fall out of self-consistency once opacity and line-driven winds are extrapolated outside the Milky Way. This is due to the fact that Fe does not scale linearly with oxygen (i.e., a proxy of a star's total metallicity), with only $\sim 30\%$ of stars with near-solar relative abundances in the local universe, and nearly none in higher redshift environments (Chrušlińska et al. 2024, 2025). Since both approaches possess limitations and validity depending on the goals of a study, we recommend that future research explicitly specifies which of the two paths is taken to ensure reproducibility.

To illustrate the effect of choosing different Z_\odot calibrations, Figure 6 shows the HR evolution of a $75 M_\odot$ star at $Z = 0.0142$ combining rotation and the application of either $Z_\odot = 0.019$ or 0.0142 for the four different models (Section 2.1.1). Evolutionary models that use inherently strong Vink et al. (2001) thin winds exhibit a high degree of sensitivity to the chosen Z_\odot value. This variability arises because the Z_\odot calibration and the inclusion of rotation act as multiplicative effects on the already high mass-loss rates, heavily impacting the star's hydrogen envelope depletion. Consequently, these strong wind models show a more robust expansion when using a higher Z_\odot (i.e., weaker mass loss) for calibration. On the other hand, weaker thin winds like Krtička et al. (2024), shown in the bottom-left panel, do not display comparable changes in evolutionary outcomes across the same parameter space.

Finally, we caution that the standard power-law scalings ($\dot{M} \propto Z^\alpha$) implicitly assume that the wind driving mechanism remains dominated by the same set of lines (primarily Fe) across all metallicities. Recent radiation-hydrodynamic studies suggest this assumption breaks down at low metallicity ($Z \leq 0.1 Z_\odot$; Krtička et al. 2025), where the dominant opacity source shifts from Fe to CNO elements. This transition introduces non-linearities in the Z -dependence that simple scaling laws cannot capture. We show its implications for mass-loss uncertainties in Section 5.

4. COOL SUPERGIANT WINDS

In isolated conditions, non-very massive stars possess insufficient luminosity to drive strong, optically thick winds during the MS. To evolve into WR stars, these objects require efficient internal mixing and strong mass loss during the cool YSG and RSG phases (Georgy et al. 2012). Current prescriptions for these phases, however, remain highly uncertain, with rates varying by orders of magnitude across different models (Antoniadis et al. 2024).

Mass loss for YSGs ($4 \text{ kK} \lesssim T_{\text{eff}} \lesssim 8 \text{ kK}$), also known as hypergiants, is highly uncertain due to few observations within this so-called “yellow void” (Nieuwenhuijzen & de Jager 1990). Additionally, both pulsations and outbursts, which cannot be self-consistently simulated in 1D, may play a more important role than continuous winds (Koumpia et al. 2020; Humphreys et al. 2023). On the other hand, RSGs ($T_{\text{eff}} \lesssim 4 \text{ kK}$) are more frequently detected and studied. Given the lack of dedicated models for the YSG phase, it is common practice to adopt for this regime the same type of mass loss that is applied to RSGs.

The initiation temperature of cool supergiant winds differs substantially between studies. Some FRANEC models initiate them at $T_{\text{eff}} \leq 12 \text{ kK}$ (Ugolini et al. 2025), encompassing blue supergiant (BSG), YSG, and RSGs. In contrast, some MESA-based models (e.g. Gilkis et al. 2021; Romagnolo et al. 2024; Liotine et al. 2025) initiate them at $T_{\text{eff}} \leq 10 \text{ kK}$, GENEC at $\log T_{\text{eff}} \leq 3.9$ (Eggenberger et al. 2021), COMPAS at $T_{\text{eff}} \leq 8 \text{ kK}$

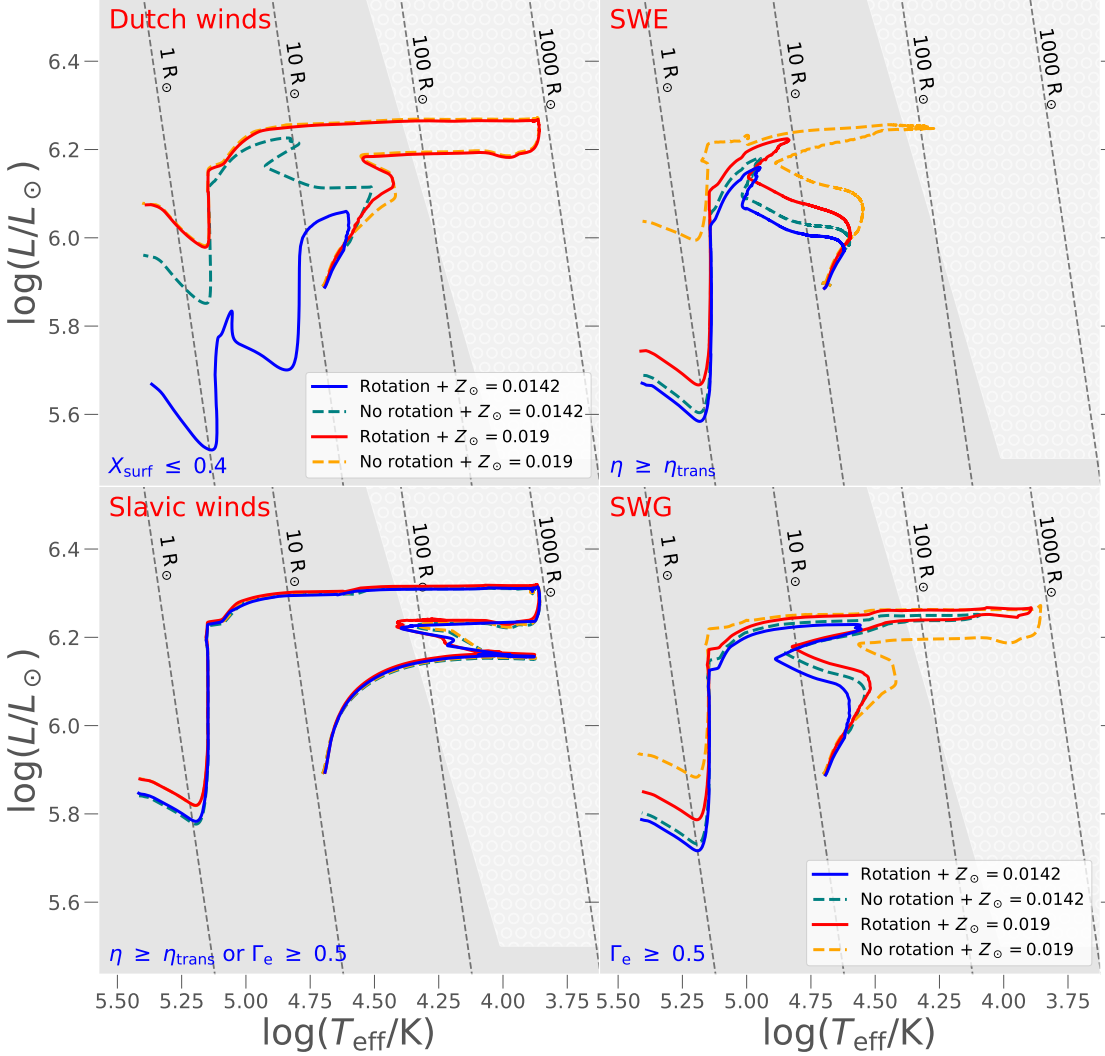


FIG. 6.—Hertzsprung-Russell (HR) diagram for the evolution of $75 M_{\odot}$ stars at $Z = 0.0142$ until the depletion of carbon in the core for four different stellar winds recipes and different transition conditions to the WR phase (see Section 3.2). Each panel shows stars with $\Omega/\Omega_{\text{crit}} = 0.4$ at ZAMS (solid lines) and non-rotating stars (dashed lines) for two values for Z_{\odot} . The LBV region beyond the HD limit is indicated (white). A higher Z_{\odot} value leads to lower mass-loss rates and to a wider expansion. With rotation, the star enters the WR phase earlier in its evolution.

(Merritt et al. 2025), and others restrict them to RSGs (e.g. Vink et al. 2021).

Following the results of Zapartas et al. (2025), the T_{eff} initiation threshold for these winds can be altered without facing strong differences within the Hertzsprung-gap (HG). This is because this phase is fast enough for mass loss to not play a substantial role. However, once stars enter the slower core-helium burning (CHeB) phase, whether cool supergiant winds are initiated or not will considerably impact their evolution.

For non-very massive stars, mass loss from optically thin winds alone is not strong enough to eject enough envelope mass to cause stars to become WR. Canonically, the widely used de Jager et al. (1988) model prescribes considerably high \dot{M} that can lead most BH progenitors at Z_{\odot} to evolve into WR stars before their collapse (Romagnolo et al. 2024). This effect could also be more evident with a higher or similar \dot{M} (van Loon et al. 2005; Goldman et al. 2017; González-Torà et al. 2023; Yang et al. 2023; González-Torà et al. 2024), while it could be weakened at lower rates (e.g. Beasor et al. 2021, 2023; Decin et al. 2024; Antoniadis et al. 2024, 2025b).

4.1. Mass loss

Mass-loss rates for cool supergiants may differ by orders of magnitude depending on which recipe is adopted, with the widest disparities arising for YSGs and beyond the HD limit.

Figure 7 shows a selected sample of cool supergiant mass-loss recipes, on top of samples based on interferometry data (González-Torà et al. 2023, 2024) and observations of low-metallicity galaxies (Christodoulou et al. 2025). The most recent studies show considerable variability in mass-loss rates, which can oscillate between comparable to the most widely used de Jager et al. (1988) ones (González-Torà et al. 2023; Yang et al. 2023; González-Torà et al. 2024), to orders of magnitude lower (Beasor et al. 2023; Antoniadis et al. 2024; Decin et al. 2024), with Beasor et al. (2023) and Decin et al. (2024) being the only two mass-loss recipes that match remarkably well between each other due to the analysis of the same supergiant sample by the respective authors. Additionally, the extrapolation to $T_{\text{eff}} > 4 \text{ kK}$ of the mass-loss rates from Antoniadis et al. (2024) would lead to underestimate mass loss, but keeping instead the temperature dependency of mass loss past

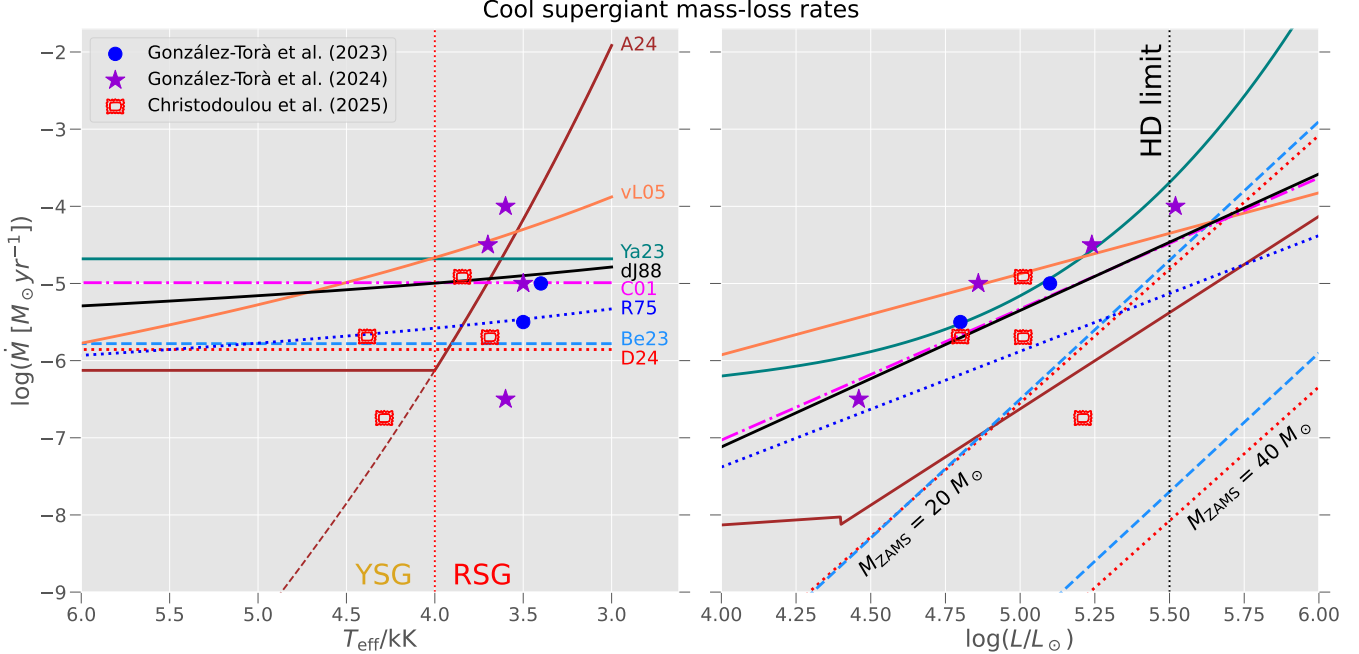


FIG. 7.— Mass-loss rates of cool supergiant winds as a function of effective temperature (left) and luminosity (right). For the left panel we adopt a constant $\log L = 5.2$, while for the right panel we assume a constant $T_{\text{eff}} = 4 \text{ kK}$. The initial mass was set to $20 M_{\odot}$ for the calculation of the mass-loss rates of [Beasor et al. \(2023\)](#) and [Decin et al. \(2024\)](#) in the left plot, and to both $20 M_{\odot}$ and $40 M_{\odot}$ for the right plot calculations. Blue circles, violet stars, and red “ravioli” symbols denote the observational measurements from [González-Torà et al. \(2023\)](#), [González-Torà et al. \(2024\)](#), and [Christodoulou et al. \(2025\)](#), respectively, and are used as independent empirical comparisons for the mass-loss prescriptions. The dashed brown line shows the [Antoniadis et al. \(2024\)](#) mass-loss relation extended beyond their observational temperature range, illustrating the behavior if mass-loss rates were not truncated at $T_{\text{eff}} = 4 \text{ kK}$. In the left panel, the vertical red dotted line marks the boundary between YSG and RSG regimes, while in the right panel the black dotted line indicates the HD limit. For both panels, the cool-supergiant mass adopted for R75 is fixed at $20 M_{\odot}$.

this threshold to a fixed $T_{\text{eff}} = 4 \text{ kK}$ shows a good agreement with what is prescribed by [Beasor et al. \(2023\)](#) and [Decin et al. \(2024\)](#).

The various recipes for cool supergiant winds can be distinguished by their primary physical dependencies. The models from [Beasor et al. \(2023\)](#) and [Decin et al. \(2024\)](#), for instance, are unique in that they are parametrized without an explicit effective temperature dependency. Instead, their mass-loss rates are a function of luminosity and M_{ZAMS} . While mass loss in these models does increase with luminosity, this trend is misleading because it is coupled with a strong inverse dependency on M_{ZAMS} , where a higher initial mass leads to considerably lower mass loss. This competing effect is so significant that in our models a star with a high initial mass of $75 M_{\odot}$, i.e., well above the most massive RSGs they used to fit their formulae ($\sim 25 M_{\odot}$), is calculated to have an extremely low mass-loss rate ($\log(\dot{M} [M_{\odot} \text{yr}^{-1}]) \approx -11$, i.e. at least six orders of magnitude than [de Jager et al. 1988](#)), despite its high luminosity. However, given the intrinsic dependency of such prescription on M_{ZAMS} , a cool supergiant forming from the merger of two stars in a binary may have considerably more mass and luminosity than an isolated star at the same T_{eff} ([Schneider et al. 2024](#)), and might lead to mass-loss rates that are orders of magnitude higher for cool supergiant winds. More generally the factor M_{ZAMS} loses meaning once stars are not in isolation, and a good practice should be to model their mass loss as a function of its current parameters, and not as an explicit function of its history. In contrast, other models incorporate a direct temperature dependence, generally showing higher mass loss at cooler temperatures. This inverse T_{eff} dependence can be expected because more evolved RSGs become cooler. The [Antoniadis et al. \(2024\)](#) recipe is a prime example, showing

a sharp increase in mass loss at low effective temperatures due to their use of a T_{eff} -relation based on the [Tabernero et al. \(2018\)](#) sample.

The extrapolation of all models past the HD limit at $\log L > 5.5$ ([Davies et al. 2018](#); [McDonald et al. 2022](#)) leads the different recipes to quickly converge to mass-loss rates similar or higher than the ones of [de Jager et al. \(1988\)](#), due to their strong dependence on luminosity. It is worth noting that while empirical power-law recipes may underestimate mass loss in this extreme regime, physical models based on convective shocks predict a “runaway” mass-loss phase for the most massive RSGs ($M_{\text{ZAMS}} \geq 30 M_{\odot}$) ([Fuller & Tsuna 2024](#)). In this scenario, as the star expands and escape velocity drops, the boil-off rate increases exponentially, potentially stripping the hydrogen envelope much faster than predicted by canonical rates (e.g., [de Jager et al. 1988](#)). This physical mechanism provides a potential solution to the scarcity of observed RSGs above a luminosity limit of $\log(L/L_{\odot}) \approx 5.5$ by naturally shortening the RSG lifetime of high-mass progenitors.

YSGs: Extrapolation to higher temperatures— Although for many stars YSG mass loss should have a limited impact in the evolution of stars ([Zapartas et al. 2025](#)), for BH progenitors this may not be the case, since at $M_{\text{ZAMS}} \gtrsim 30 M_{\odot}$, CHeB, when mass loss can considerably affect the envelope evolution, is initiated at $T_{\text{eff}} > 4 \text{ kK}$, i.e. during the YSG phase. Many of the mass-loss recipes for cool supergiant winds do not have any T_{eff} dependency at all, which may lead to several uncertainties when applied to evolutionary models, even more for binary systems, where interactions among stars can drastically affect their HR position (e.g., [Dutta & Klencki 2024](#)).

5. DISCUSSION: OTHER MASS-LOSS UNCERTAINTIES

The modeling of mass loss in stellar evolution is subject to several more key uncertainties, a selected list below.

Fe and CNO driving limits— Standard mass-loss prescriptions rely on fits from atmospheric models based on Fe spectral lines that provide the necessary opacity to drive the wind. Recent hydrodynamically consistent modeling has identified a critical metallicity threshold, below which this driving mechanism fails. Below a metallicity of roughly the Small Magellanic Cloud (SMC) value of $0.2 Z_{\odot}$, the Fe opacity peak becomes insufficient to drive the wind (Krtička et al. 2025). This transition introduces significant uncertainties: while some models predict a shallow decline in mass loss ($\dot{M} \propto Z^{0.42}$; Vink & Sander 2021) due to CNO efficiency, others predict a steep drop ($\dot{M} \propto Z^{1.4}$) as the wind becomes lacking of driving lines (Krtička et al. 2025). This discrepancy, summarized in Table 3, highlights a fundamental breakdown in the application of standard wind recipes. Current evolutionary codes typically extrapolate mass-loss rates to low metallicities using simple power-law scalings calibrated on Galactic (Fe-driven) winds. This approach implicitly assumes that the wind-driving mechanism remains dominated by the same set of ions throughout cosmic history. In the intermediate regime ($0.1 < Z/Z_{\odot} < 0.2$), the driving is neither purely Fe-based nor purely CNO-based; instead, α -elements such as Silicon (Si) combined with CNO elements become the primary drivers, driving the mass-loss rates of e.g. WN stars down by roughly two orders of magnitude from the SMC levels (Sander et al. 2020). Extrapolating Fe-based formulations here ignores the specific influence of Si/CNO. As metallicity falls further to the CNO regime ($Z \sim 0.01 Z_{\odot}$), the statistical forest of overlapping Fe lines disappears entirely, leaving the wind to be driven by a few discrete CNO lines. By applying a Galactic Fe-scaling to these regimes, models force a "strong wind" physics onto a "weak wind" environment. Therefore, we argue that mass-loss descriptions must move beyond simple Z -dependent scalars and adopt species-dependent driving limits.

TABLE 3

MAIN DRIVERS OF THIN AND THICK WINDS AS A FUNCTION OF METALLICITY

Z regime	$\sim Z/Z_{\odot}$	Driver	Key reference
Galactic	1.0 ^a	Fe	Abbott (1982)
SMC	0.2	Fe + CNO	Sander et al. (2020)
Fe limit	0.1	Si + CNO	Krtička et al. (2025)
Very low Z	0.01	CNO	Krtička & Kubát (2009)
Primordial	0	Continuum?	Krtička & Kubát (2006)

^aArbitrary approximation for the Milky Way metallicity distribution.

Inflation— Envelope inflation is a rapid, non-thermal-equilibrium increase in the stellar radius, and represents a major uncertainty in massive star evolution. It is driven by near-surface layers approaching the Eddington limit, a process linked to opacity peaks from Fe or He ionization (Cantiello et al. 2009; Jermyn et al. 2022). While its underlying physics is not fully understood, inflation causes numerical instabilities in 1D models (Agrawal et al. 2022). To mitigate this, ad-hoc solutions such as the *use_superad_reduction* or *MLT++* modules in MESA are used, but this effectively alters the effective temperature by lowering temperature gradients, thereby

affecting the predicted mass-loss rates and wind types. Despite this measure, inflation still occurs in some models, and the astrophysical reality of this phenomenon, along with the justification for such "stellar engineering" solutions (e.g. Jiang et al. 2015), remains debated. Regardless, the interplay between inflation and stellar winds is currently poorly understood, suggesting a need for further corrections to mass loss or the development of ad-hoc models.

Internal mixing and rotation— Internal mixing plays an important role in the structural evolution of massive stars, even more so when rotation is included and potentially enhanced by tidal interactions with a stellar companion. This leads first to rotationally-enhanced mass-loss rates, and also to a more chemically homogeneous structure of the envelope, hence different HR positions. Gilkis et al. (2021) showed how rotating stars, even at Z_{\odot} , can reach sufficiently high internal mixing to keep stars chemically homogeneous and therefore making them unable to expand past the HD limit. However, it must be highlighted that, at least at near-solar metallicity, recent models show that winds dominate the evolution of very massive stars due to their high mass loss, and internal mixing does not play a significant role (e.g., Romagnolo et al. 2024). This is because the winds within this regime are strong enough to eject most angular momentum in the early evolutionary stages. On the other hand, there is strong observational evidence to support the concept that rotational mixing is considerably more efficient at lower metallicities (Martins et al. 2024).

LBV winds— In the treatment of evolved massive stars, eruptive mass loss, which can be for instance inferred by the presence of dusty RSGs with low mass-loss rates (Christodoulou et al. 2025), is often modeled with ad-hoc LBV prescriptions. Some traditional LBV formulations come from Hurley et al. (2000), which increases mass-loss rates by an additive factor $\dot{M}_{\text{LBV}} \propto (R\sqrt{L} - 1)^3 (L/(6 \times 10^{-5}) - 1)$ beyond the HD limit, or the Belczynski et al. (2010) approach, which applies a fixed mass loss of $f_{\text{LBV}} \times 10^{-4} M_{\odot} \text{yr}^{-1}$ for the same HR regime, with f_{LBV} a calibrated factor usually around unity. While computationally efficient, these methods lack a dependence on the star's internal energy budget and rely on calibrations that predate modern observational and theoretical constraints. In contrast, the recent formulation by Cheng et al. (2024), as well as the more canonical super-Eddington FRANEC formulation (Limongi & Chieffi 2018), triggers eruptive mass loss in 1D models by identifying and ejecting envelope layers where the opacity-driven luminosity exceeds the local Eddington limit. This mechanism may naturally reproduce the absence of red supergiants above $\sim 25 M_{\odot}$ without relying on arbitrary stability thresholds, but also represents physics that overlaps with the phenomenon of inflation, leading to further uncertainties on which regime the two phenomena dominate.

Mass-loss peaks and interpolation— Transitions between different mass-loss schemes in 1D stellar models, such as the onset of cool supergiant winds, the bistability jump, or the switch to optically thick winds, often create artificial jumps in mass-loss rates. These discontinuities arise because individual formulae, from different studies, are calibrated for specific stellar types and are not designed to connect smoothly, though some jumps are intentional (see e.g. the Vink et al. 2001 bistability jump formulation). Interpolation schemes are often adopted to smooth these transitions and avoid numerical noise from abruptly changing mass-loss rates. These computational

solutions are an accepted limitation of 1D evolutionary codes, which are intended to approximate stellar evolution under an acceptable degree rather than mirror first-principle physics.

Mass-loss peaks and maximization— Many models do not adopt interpolation methods to transition between different mass-loss recipes, but instead parametrize mass-loss rates as the maximum value between two or more stellar winds recipes at a given timestep. For instance, many GENEC models (see e.g. Eggenberger et al. 2008; Hirschi et al. 2025) define mass loss for WNL stars as the maximum value between Vink et al. (2001) and Gräfener & Hamann (2008). This ensures numerical stability, since usually numerical errors are more frequent with jumps in mass-loss rates or in general with more massive envelopes, and avoids the underestimation of mass loss from extrapolation. On the other hand, maximizing mass loss between two or more formulations breaks consistency with the original fits and does not necessarily represent the strength of stellar winds. The recipe that produces stronger mass loss is not necessarily the right one, and this method risks to lead to mass-loss overestimation. Whether the switch between two or more mass-loss formulations is done by linear interpolation or by taking the highest mass-loss value, stellar models lose self-consistency in favor of computational efficiency and a smoother mass-loss history.

Massive stars in binaries and multiples— Massive stars are not usually born as isolated entities, but with at least one stellar companion (Sana et al. 2012; Moe & Di Stefano 2017). On top of that, within the M_{ZAMS} regime of BH progenitors it was shown by both theoretical and observational works that most of these stars reside in systems with more than two stellar components (Offner et al. 2023; Bordier et al. 2024; de Sá et al. 2024). Many massive stars do not therefore evolve in isolation, and their overall evolution will be affected by their stellar companion(s). Both mass transfer (Renzo et al. 2023; Landri & Pejcha 2024) and supernova (Ogata et al. 2021; Hirai 2023) events may considerably alter the binding energy within stellar envelopes, as well as their mass, mean molecular weight, and consequently their surface properties. This is likely to considerably impact mass loss, resulting in a non-negligible deviation from the modeled isolated evolution of the star. Furthermore, in systems hosting a neutron star, energetic pulsar winds can irradiate and ablate the companion’s envelope—a process essential for shaping the evolution of spider binaries—thereby driving mass-loss rates that are entirely distinct from standard stellar winds (e.g., Chen et al. 2013; Benvenuto et al. 2014; Misra et al. 2025). All these effects represent further evidence that η_{trans} should not be a fixed factor at a given metallicity that is calculated from hypothetical chemically homogeneous conditions, but a value that can considerably vary and should be calculated following the *current* surface conditions of a star (see more in Section 3.2.2). Similarly, the existence of these binary interactions imply that the M_{ZAMS} dependency of the mass-loss rates from Beasor et al. (2023) and Decin et al. (2024) limits their applicability to only single stars below the HD limit.

Magnetic fields— About 4-10% of the observed O-type stars were shown to have strong magnetic fields that likely do not come from dynamo effects, but are a relic from an event or an evolutionary stage that occurred earlier in their past (Petit et al. 2019). Additionally, at least a fraction of very massive stars likely comes from mergers during the pre- or early-MS phase. Such merger events are postulated to create strong

dynamo effects (Wickramasinghe et al. 2014), with recent 3D hydrodynamical simulations suggesting that these mergers are a highly efficient channel for generating strong, stable magnetic fields (Vynatheya et al. 2025). Regardless of the formation pathway for their magnetic fields, magnetic stars represent a vastly unexplored field in stellar evolution. Strong magnetic fields quench mass loss by effectively adding to the gravitational pull that keeps stellar surfaces bound, increase angular momentum loss via magnetic braking, and affect the transport of angular momentum and elements within stellar interiors (Keszthelyi et al. 2022).

Pop II and Pop III— In the primordial regime where even CNO driving is absent, the dominant mass-loss mechanism must fundamentally shift from radiation-driven to rotationally-driven or continuum-driven processes. For Population II (extremely metal-poor) and Population III (metal-free) stars, the (near-)lack of opacity implies that line-driven winds are negligible, though free-electron (Thomson) scattering may still contribute to mass loss near the Eddington limit. Consequently, rotationally-driven mechanical mass loss, which is distinct from the rotational wind mass-loss enhancement currently adopted in evolutionary models (e.g., Friend & Abbott 1986; Langer 1998; Maeder & Maeynet 2000), may become the primary channel for mass ejection (rotation reduces the equatorial gravitational pull, which relaxes the L/M ratio, and therefore increasing the Eddington factor Γ_e). While models usually set the break-up surface angular momentum threshold around 98% of the critical value (Meynet et al. 2006), we argue that mass loss may be initiated considerably earlier. Standard 1D evolutionary models operate under hydrostatic equilibrium that explicitly neglects the radial inertial term in the momentum equation. By defining the critical limit purely through static force balance rather than a hydrodynamic launch condition, these models essentially visualize the stellar surface as “static” even at breakup. This approximation ignores the dynamic pressure of the outflow and the complex effects of turbulence (e.g., Kee et al. 2021), which can establish a non-zero velocity baseline and effectively lower the angular momentum threshold for mass shedding. Consequently, the implementation of mechanical mass loss in 1D simulations often represents a numerical compromise rather than a resolved physical process. Codes typically employ algorithmic “patches”, such as implicit mass-loss boosts (Ekström et al. 2008), that instantaneously remove mass and angular momentum to force the star to remain sub-critical. This zero-velocity visualization fails to capture the anisotropy of the outflow, where mass loss likely manifests differently at the pole and the equator, as well as potentially underestimating the terminal velocity of stellar material from the surface.

Pulsations— Pulsational instabilities are not usually included in standard mass-loss formulations for massive stars. While 1D stellar evolution codes like MESA can be coupled with linear pulsation modules such as GYRE (Townsend & Teitler 2013) to identify unstable modes, these tools are limited to linear stability analysis. They cannot self-consistently predict the non-linear saturation amplitudes required to determine mass fluxes. Consequently, accurately resolving pulsation-driven mass loss requires full 3D radiation-hydrodynamics simulations to capture the associated shocks and turbulence (Jiang et al. 2015; Freytag et al. 2017; Jiang et al. 2018), or the use of 1D modules that approximate these effects, such as turbulent pressure models (Fuller & Tsuna 2024) or phenomenological

prescriptions like those of [Yoon & Cantiello \(2010\)](#).

6. CONCLUSIONS

In this work we have presented a systematic comparative analysis of the stellar wind prescriptions widely used in modern stellar evolution codes for massive stars. By examining the three primary mass-loss regimes (optically thin line-driven winds, optically thick Wolf-Rayet winds, and cool supergiant winds) we have highlighted the deep and often contradictory assumptions embedded in current models. The choice of a specific mass-loss recipe is not a minor implementation detail but a dominant source of uncertainty that fundamentally shapes the predicted evolution of massive stars.

Our key findings reveal significant, and in some cases irreconcilable, discrepancies across all investigated mass-loss regimes:

- Optically thin winds: We find that the predicted mass-loss rates can differ by more than an order of magnitude depending on the chosen prescription. The treatment of wind clumping and the existence, strength, and temperature location of the bistability jump(s) remain major points of contention, leading to vastly different mass-loss histories even for identical stars.
- Optically thick winds: We identified critical flaws in the criteria used to trigger the formation of a Wolf-Rayet star. We show that the commonly used Eddington factor Γ_e may act as an inconsistent proxy for the initiation of optically thick winds, if applied outside its domain of validity. Furthermore, we demonstrate that the alternative multi-scattering η criterion for wind efficiency is highly model-dependent, and that its current implementation in evolutionary codes sacrifices consistency with a star's instantaneous surface properties to artificially anchor the model to the input requirements of the [Vink et al. \(2011\)](#) parameterization. To address this, we provide recommendations for improving the multi-scattering criterion and introduce a new, model-agnostic framework for this transition. By calculating wind efficiency and escape velocities based on the star's current physical state rather than hypothetical chemically homogeneous conditions, this flexible approach ensures greater physical consistency across the mass spectrum.
- Cool supergiant winds: The landscape of available prescriptions is equally divergent. Recent models based on new observational constraints predict mass-loss rates

that can be orders of magnitude lower than the canonical prescriptions traditionally used in stellar evolution, but with similar or even higher mass loss than legacy models at $\log(L/L_\odot) > 5.5$, i.e. the extrapolation regime past the Humphrey-Davidson limit.

We also introduce the "cool Wolf-Rayet problem", a regime for which no dedicated, physically consistent model currently exists. Consequently, models must employ ad-hoc workarounds. For instance, some models extrapolate weaker optically thin winds into this cooler domain ([Romagnolo et al. 2024](#); [Gormaz-Matamala et al. 2025a](#)), which is more justified by recent theoretical studies ([Bernini-Peron et al. 2025](#); [Lefever et al. 2025](#)) while others adopt stronger, optically thick wind prescriptions calibrated from warmer Wolf-Rayet stars ([Glebbeek et al. 2009](#); [Sabahhit et al. 2023](#)), which instead better respects the Humphrey-Davison limit ([Boco et al. 2025](#)). The uncertainty extends to the transition criteria themselves. The use of Γ_e -dependent physics is formally valid only for fully ionized plasmas where electron scattering dominates, a condition met at effective temperatures $T_{\text{eff}} \geq 30$ kK, with a potential approximated extension down to 15 kK due to the still relatively strong contribution of free-electron scattering. Below this threshold, the recombination of hydrogen and helium contributes considerably to the opacity, and the physical basis for the classical Γ_e calculation collapses. Applying transition criteria and mass-loss rates based on the classical Γ_e in this regime is a fundamental flaw that forces models to rely on uncertain extrapolations rather than a self-consistent physical framework.

CODE CITATIONS

This work used the following software packages: `matplotlib` ([Hunter 2007](#)), `numpy` ([Harris et al. 2020](#)), and `pasta-marker` ([PASTA Collaboration 2024, 2025](#)).

The MESA models used are available at github.com/AmedeoRom/Stellar_Winds_Atlas

ACKNOWLEDGEMENTS

AR acknowledges financial support from the European Research Council for the ERC Consolidator grant DEMOBLACK, under contract no. 770017 and from the German Excellence Strategy via the Heidelberg Cluster of Excellence (EXC 2181 - 390900948) STRUCTURES. ACGM thanks the support from project 10108195 MERIT (MSCA-COFUND Horizon Europe). Computations for this article have been performed using the computer cluster at CAMK PAN. The authors thank Cristiano Ugolini, Lucas M. de Sá, Gemma Gonzalez i Tora, JD Merritt, Lumen Boco, Gautham Sabahhit, Michela Mapelli, Emmanouil Zapartas, Andreas Sander, Earl Bellinger, Radek Smolec, Sylvia Ekström, and Jiří Krtička for their feedback and the constructive discussions.

REFERENCES

Aadland, E., Massey, P., Hillier, D. J., et al. 2022, *ApJ*, 931, 157

Abbott, D. C. 1982, *ApJ*, 259, 282

Agrawal, P., Hurley, J., Stevenson, S., Szécsi, D., & Flynn, C. 2020, *Monthly Notices of the Royal Astronomical Society*, 497, 4549–4564

Agrawal, P., Szécsi, D., Stevenson, S., Eldridge, J. J., & Hurley, J. 2022, *MNRAS*, 512, 5717

Alkousa, T., Crowther, P. A., Bestenlehner, J. M., et al. 2025, arXiv e-prints, arXiv:2506.09129

Anders, E., & Grevesse, N. 1989, *Geochim. Cosmochim. Acta*, 53, 197

Andrews, J. J., Bawera, S. S., Briel, M., et al. 2024, arXiv e-prints, arXiv:2411.02376

Antoniadis, K., Bonanos, A. Z., de Wit, S., et al. 2024, *A&A*, 686, A88

—. 2025a, *A&A*, 695, C2

Antoniadis, K., Zapartas, E., Bonanos, A. Z., et al. 2025b, *A&A*, 702, A178

Arroyo-Torres, B., Wittkowski, M., Chiavassa, A., et al. 2015, *A&A*, 575, A50

Asplund, M., Grevesse, N., Sauval, A. J., & Scott, P. 2009, *ARA&A*, 47, 481

Backs, F., Brands, S. A., de Koter, A., et al. 2024, *A&A*, 692, A88

Banerjee, S., Belczynski, K., Fryer, C. L., et al. 2020, *A&A*, 639, A41

Bavera, S. S., Fragos, T., Zapartas, E., et al. 2023, *Nature Astronomy*, 7, 1090

Beasor, E. R., Davies, B., & Smith, N. 2021, *ApJ*, 922, 55

Beasor, E. R., Davies, B., Smith, N., et al. 2023, *MNRAS*, 524, 2460

Belczynski, K., Dominik, M., Bulik, T., et al. 2010, *The Astrophysical Journal*, 715, L138–L141

Belczynski, K., Romagnolo, A., Olejak, A., et al. 2022, *ApJ*, 925, 69

Benvenuto, O. G., De Vito, M. A., & Horvath, J. E. 2014, *ApJ*, 786, L7

Bernini-Peron, M., Marcolino, W. L. F., Sander, A. A. C., et al. 2023, *A&A*, 677, A50

Bernini-Peron, M., Sander, A. A. C., Ramachandran, V., et al. 2024, *A&A*, 692, A89

Bernini-Peron, M., Sander, A. A. C., Najarro, F., et al. 2025, *A&A*, 697, A41

Bestenlehner, J. M. 2020, *MNRAS*, 493, 3938

Bestenlehner, J. M., Gräfener, G., Vink, J. S., et al. 2014, *A&A*, 570, A38

Björklund, R., Sundqvist, J. O., Puls, J., & Najarro, F. 2021, *A&A*, 648, A36

Björklund, R., Sundqvist, J. O., Singh, S. M., Puls, J., & Najarro, F. 2023, *A&A*, 676, A109

Boco, L., Mapelli, M., Sander, A. A. C., et al. 2025, arXiv e-prints, arXiv:2507.00137

Bodensteiner, J., Shenar, T., Mahy, L., et al. 2020, *A&A*, 641, A43

Bordier, E., de Wit, W. J., Frost, A. J., et al. 2024, *A&A*, 681, A85

Bouret, J. C., Lanz, T., & Hillier, D. J. 2005, *A&A*, 438, 301

Brands, S. A., de Koter, A., Bestenlehner, J. M., et al. 2022, *A&A*, 663, A36

Breivik, K., Coughlin, S., Zevin, M., et al. 2020, *ApJ*, 898, 71

Cantiello, M., Langer, N., Brott, I., et al. 2009, *A&A*, 499, 279

Castor, J. I., Abbott, D. C., & Klein, R. I. 1975, *ApJ*, 195, 157

Chen, H.-L., Chen, X., Tauris, T. M., & Han, Z. 2013, *ApJ*, 775, 27

Cheng, S. J., Goldberg, J. A., Cantiello, M., et al. 2024, arXiv e-prints, arXiv:2405.12274

Christodoulou, E., de Wit, S., Bonanos, A. Z., et al. 2025, arXiv e-prints, arXiv:2510.26674

Chrušlińska, M., Curti, M., Pakmor, R., et al. 2025, arXiv e-prints, arXiv:2511.15782

Chrušlińska, M., Pakmor, R., Matthee, J., & Matsuno, T. 2024, *A&A*, 686, A186

Clark, J. S., Najarro, F., Negueruela, I., et al. 2012, *A&A*, 541, A145

Costa, G., Bressan, A., Mapelli, M., et al. 2021, *MNRAS*, 501, 4514

Costa, G., Shepherd, K. G., Bressan, A., et al. 2025, *A&A*, 694, A193

Crowther, P. A. 2001, in *Astrophysics and Space Science Library*, Vol. 264, The Influence of Binaries on Stellar Population Studies, ed. D. Vanbeveren, 215

Crowther, P. A. 2007, *ARA&A*, 45, 177

Crowther, P. A., Lennon, D. J., & Walborn, N. R. 2006, *A&A*, 446, 279

Crowther, P. A., Schnurr, O., Hirschi, R., et al. 2010, *MNRAS*, 408, 731

Davidson, K. 1987, *ApJ*, 317, 760

Davies, B., Crowther, P. A., & Beasor, E. R. 2018, *MNRAS*, 478, 3138

de Burgos, A., Keszthelyi, Z., Simón-Díaz, S., & Urbaneja, M. A. 2024, *A&A*, 687, L16

de Jager, C., Nieuwenhuijzen, H., & van der Hucht, K. A. 1988, *A&As*, 72, 259

de Sá, L. M., Bernardo, A., Rocha, L. S., Bachega, R. R. A., & Horvath, J. E. 2024, *MNRAS*, 535, 2019

Decin, L., Richards, A. M. S., Marchant, P., & Sana, H. 2024, *A&A*, 681, A17

Dorozsmai, A., & Toonen, S. 2024, *MNRAS*, 530, 3706

Dray, L. M., & Tout, C. A. 2003, *MNRAS*, 341, 299

Dray, L. M., Tout, C. A., Karakas, A. I., & Lattanzio, J. C. 2003, *MNRAS*, 338, 973

Drout, M. R., Götberg, Y., Ludwig, B. A., et al. 2023, *Science*, 382, 1287

Dutta, D., & Klencki, J. 2024, *A&A*, 687, A215

Eddington, A. S. 1926, The Internal Constitution of the Stars

Eggenberger, P., Meynet, G., Maeder, A., et al. 2008, *ApSS*, 316, 43

Eggenberger, P., Ekström, S., Georgy, C., et al. 2021, *A&A*, 652, A137

Ekström, S., Meynet, G., Maeder, A., & Barblan, F. 2008, *A&A*, 478, 467

El-Badry, K., Seeburger, R., Jayasinghe, T., et al. 2022, *MNRAS*, 512, 5620

Eldridge, J. J., & Vink, J. S. 2006, *A&A*, 452, 295

Farmer, R., Laplace, E., de Mink, S. E., & Justham, S. 2021, *ApJ*, 923, 214

Field, G. B. 1974, *ApJ*, 187, 453

Freytag, B., Liljegegren, S., & Höfner, S. 2017, *A&A*, 600, A137

Friend, D. B., & Abbott, D. C. 1986, *ApJ*, 311, 701

Fuller, J., & Tsuna, D. 2024, The Open Journal of Astrophysics, 7, 47

Garcia, M., Fullerton, A. W., Najarro, F., et al. 2025, The Astrophysical Journal Letters, 990, L23

Georgy, C., Ekström, S., Meynet, G., et al. 2012, *A&A*, 542, A29

Gilkis, A., Laplace, E., Arcavi, I., Shenar, T., & Schneider, F. R. N. 2025, *MNRAS*, 540, 3094

Gilkis, A., & Mazeh, T. 2024, Gaia BH1 and BH2 – Evolutionary Models with Overshooting of the Black Hole Progenitors within the Present-Day Binary Separation, arXiv:2409.15899

Gilkis, A., Shenar, T., Ramachandran, V., et al. 2021, *MNRAS*, 503, 1884

Glebbeek, E., Gaburov, E., de Mink, S. E., Pols, O. R., & Portegies Zwart, S. F. 2009, *A&A*, 497, 255

Goldman, S. R., van Loon, J. T., Zijlstra, A. A., et al. 2017, *MNRAS*, 465, 403

González-Torà, G., Wittkowski, M., Davies, B., & Plez, B. 2024, *A&A*, 683, A19

González-Torà, G., Wittkowski, M., Davies, B., Plez, B., & Kravchenko, K. 2023, *A&A*, 669, A76

Gormaz-Matamala, A. C., Cuadra, J., Ekström, S., et al. 2024, *A&A*, 687, A290

Gormaz-Matamala, A. C., Cuadra, J., Kubátová, B., Kubát, J., & Ekström, S. 2025b, arXiv e-prints, arXiv:2512.07432

Gormaz-Matamala, A. C., Cuadra, J., Meynet, G., & Curé, M. 2023, *A&A*, 673, A109

Gormaz-Matamala, A. C., Curé, M., Hillier, D. J., et al. 2021, *ApJ*, 920, 64

Gormaz-Matamala, A. C., Curé, M., Lobel, A., et al. 2022a, *A&A*, 661, A51

Gormaz-Matamala, A. C., Curé, M., Meynet, G., et al. 2022b, *A&A*, 665, A133

Gormaz-Matamala, A. C., Romagnolo, A., & Belczynski, K. 2025a, *A&A*, 696, A72

Götberg, Y., Drout, M. R., Ji, A. P., et al. 2023, *ApJ*, 959, 125

Gräfener, G. 2021, *A&A*, 647, A13

Gräfener, G., & Hamann, W. R. 2008, *A&A*, 482, 945

Gräfener, G., Owocki, S. P., Grassitelli, L., & Langer, N. 2017, *A&A*, 608, A34

Gräfener, G., Vink, J. S., de Koter, A., & Langer, N. 2011, *A&A*, 535, A56

Grevesse, N., Noels, A., & Sauval, A. J. 1996, in *Astronomical Society of the Pacific Conference Series*, Vol. 99, Cosmic Abundances, ed. S. S. Holt & G. Sonneborn, 117

Hamann, W. R., & Koesterke, L. 1998, *A&A*, 335, 1003

Harris, C. R., Millman, K. J., van der Walt, S. J., et al. 2020, *Nature*, 585, 357

Heger, A., Langer, N., & Woosley, S. E. 2000, *ApJ*, 528, 368

Heger, A., Woosley, S. E., & Spruit, H. C. 2005, *ApJ*, 626, 350

Hendriks, D. D., van Son, L. A. C., Renzo, M., Izzard, R. G., & Farmer, R. 2023, *MNRAS*, 526, 4130

Higgins, E. R., Vink, J. S., Hirschi, R., Laird, A. M., & Sabhahit, G. N. 2023, *MNRAS*, 526, 534

Hirai, R. 2023, *MNRAS*, 523, 6011

Hirschi, R., Goodman, K., Meynet, G., et al. 2025, arXiv e-prints, arXiv:2508.21233

Höfner, S., Gautschy-Loidl, R., Aringer, B., & Jørgensen, U. G. 2003, *A&A*, 399, 589

Höfner, S., & Olofsson, H. 2018, *A&A Rev.*, 26, 1

Hoyle, F., & Wickramasinghe, N. C. 1962, *Monthly Notices of the Royal Astronomical Society*, 124, 417

Humphreys, R. M., & Davidson, K. 1979, *ApJ*, 232, 409

—. 1994, *Publications of the Astronomical Society of the Pacific*, 106, 1025

Humphreys, R. M., Jones, T. J., & Martin, J. C. 2023, *The Astronomical Journal*, 166, 50

Hunter, J. D. 2007, *Computing in Science & Engineering*, 9, 90

Hurley, J. R., Pols, O. R., & Tout, C. A. 2000, *Monthly Notices of the Royal Astronomical Society*, 315, 543

Iorio, G., Mapelli, M., Costa, G., et al. 2023, *MNRAS*, 524, 426

Irrgang, A., Geier, S., Kreuzer, S., Pelisoli, I., & Heber, U. 2020, *A&A*, 633, L5

Jermyn, A. S., Anders, E. H., Lecoanet, D., & Cantiello, M. 2022, *ApJs*, 262, 19

Jermyn, A. S., Bauer, E. B., Schwab, J., et al. 2023, *The Astrophysical Journal Supplement Series*, 265, 15

Jiang, Y.-F., Cantiello, M., Bildsten, L., Quataert, E., & Blaes, O. 2015, *ApJ*, 813, 74

Jiang, Y.-F., Cantiello, M., Bildsten, L., et al. 2018, *Nature*, 561, 498

Josiek, J., Ekström, S., & Sander, A. A. C. 2024, arXiv e-prints, arXiv:2404.14488

Kamlah, A. W. H., Leveque, A., Spurzem, R., et al. 2022, *MNRAS*, 511, 4060

Kee, N. D., Sundqvist, J. O., Decin, L., de Koter, A., & Sana, H. 2021, *A&A*, 646, A180

Keszthelyi, Z., Brands, S. A., de Koter, A., Langer, N., & Puls, J. 2025, arXiv e-prints, arXiv:2506.15230

Keszthelyi, Z., de Koter, A., Götberg, Y., et al. 2022, *MNRAS*, 517, 2028

Klencki, J., Nelemans, G., Istrate, A. G., & Pols, O. 2020, *A&A*, 638, A55

Köhler, K., Langer, N., de Koter, A., et al. 2015, *A&A*, 573, A71

Koumpia, E., Oudmaijer, R. D., Graham, V., et al. 2020, *A&A*, 635, A183

Krtička, J., & Kubát, J. 2006, *A&A*, 446, 1039

—. 2009, *A&A*, 493, 585

—. 2017, *A&A*, 606, A31

Krtička, J., Kubát, J., & Krtičková, I. 2025, arXiv e-prints, arXiv:2508.21702

Krtička, J., Kubát, J., & Krtičková, I. 2021, *A&A*, 647, A28

—. 2024, *A&A*, 681, A29

Kruckow, M. U., Andrews, J. J., Fragos, T., et al. 2024, *A&A*, 692, A141

Kudritzki, R. P., Paudlach, A., & Puls, J. 1987, *A&A*, 173, 293

Kudritzki, R.-P., & Puls, J. 2000, *ARA&A*, 38, 613

Lai, E. V., De Marco, B., Zdziarski, A. A., et al. 2022, *MNRAS*, 512, 2671

Lai, E. V., De Marco, B., Cavecchi, Y., et al. 2024, *A&A*, 691, A78

Lamers, H. J. G. L. M., & Cassinelli, J. P. 1999, *Introduction to Stellar Winds*

Lamers, H. J. G. L. M., Snow, T. P., & Lindholm, D. M. 1995, *ApJ*, 455, 269

Landri, C., & Pejcha, O. 2024, *MNRAS*, 531, 3391

Langer, N. 1998, *A&A*, 329, 551

Langer, N., Kiriakidis, M., El Eid, M. F., Fricke, K. J., & Weiss, A. 1988, *A&A*, 192, 177

Ledoux, P. 1947, *ApJ*, 105, 305

Lefever, R. R., Sander, A. A. C., Bernini-Peron, M., et al. 2025, *A&A*, 700, A2

Limongi, M., & Chieffi, A. 2006, *ApJ*, 647, 483

Limongi, M., & Chieffi, A. 2018, *The Astrophysical Journal Supplement Series*, 237, 13

Liotine, C., Kalogera, V., Andrews, J. J., et al. 2025, *ApJ*, 982, 53

Lucy, L. B., & Solomon, P. M. 1970, *ApJ*, 159, 879

Maeder, A. 1983, *A&A*, 120, 113

Maeder, A., & Maeynet, G. 2000, *Annual Review of Astronomy and Astrophysics*, 38, 143

Markova, N., & Puls, J. 2008, *A&A*, 478, 823

Martinet, S., Meynet, G., Ekström, S., Georgy, C., & Hirschi, R. 2023, *A&A*, 679, A137

Martinet, S., Meynet, G., Nandal, D., et al. 2022, *A&A*, 664, A181

Martins, F., & Palacios, A. 2022, *A&A*, 659, A163

Martins, F., Schaerer, D., Hillier, D. J., et al. 2005, *A&A*, 441, 735

Martins, F., Bouret, J.-C., Hillier, D. J., et al. 2024, *A&A*, 689, A31

McDonald, S. L. E., Davies, B., & Beasor, E. R. 2022, *MNRAS*, 510, 3132

Merritt, J., Stevenson, S., Sander, A., et al. 2025, arXiv e-prints, arXiv:2507.17052

Meynet, G., Ekström, S., & Maeder, A. 2006, *A&A*, 447, 623

Meynet, G., & Maeder, A. 2003, *A&A*, 404, 975

Meynet, G., Maeder, A., Schaller, G., Schaerer, D., & Charbonnel, C. 1994, *Å&As*, 103, 97

Misra, D., Linares, M., & Ye, C. S. 2025, *A&A*, 693, A314

Moe, M., & Di Stefano, R. 2017, *ApJs*, 230, 15

Nathaniel, K., Langer, N., Simón-Díaz, S., et al. 2025, *A&A*, 702, A197

Neilson, H. R., & Lester, J. B. 2008, *ApJ*, 684, 569

Nieuwenhuijzen, H., & de Jager, C. 1990, *A&A*, 231, 134

Nugis, T., & Lamers, H. J. G. L. M. 2000, *A&A*, 360, 227

Offner, S. S. R., Moe, M., Kratter, K. M., et al. 2023, in *Astronomical Society of the Pacific Conference Series*, Vol. 534, *Protostars and Planets VII*, ed. S. Inutsuka, Y. Aikawa, T. Muto, K. Tomida, & M. Tamura, 275

Ogata, M., Hirai, R., & Hijikawa, K. 2021, *MNRAS*, 505, 2485

Owocki, S. P. 2015, in *Astrophysics and Space Science Library*, Vol. 412, *Very Massive Stars in the Local Universe*, ed. J. S. Vink, 113

Paczynski, B., & Proszynski, M. 1986, *ApJ*, 302, 519

PASTA Collaboration. 2024, arXiv e-prints, arXiv:2403.20314

—. 2025, arXiv e-prints, arXiv:2503.23126

Pauldrach, A., Puls, J., & Kudritzki, R. P. 1986, *A&A*, 164, 86

Pauldrach, A. W. A., & Puls, J. 1990, *A&A*, 237, 409

Pauli, D., Oskinova, L. M., Hamann, W. R., et al. 2025, *A&A*, 697, A114

Paxton, B., Bildsten, L., Dotter, A., et al. 2011, *ApJs*, 192, 3

Paxton, B., Cantiello, M., Arras, P., et al. 2013, *The Astrophysical Journal Supplement Series*, 208, 4

Paxton, B., Marchant, P., Schwab, J., et al. 2015, *ApJs*, 220, 15

Paxton, B., Schwab, J., Bauer, E. B., et al. 2018, *ApJs*, 234, 34

Paxton, B., Smolec, R., Schwab, J., et al. 2019, *ApJs*, 243, 10

Petit, V., Wade, G. A., Schneider, F. R. N., et al. 2019, *Monthly Notices of the Royal Astronomical Society*, 489, 5669

Puls, J., Vink, J. S., & Najarro, F. 2008, *Astronomy and Astrophysics Review*, 16, 209

Reimers, D. 1975, *Memoires of the Societe Royale des Sciences de Liege*, 8, 369

Renzo, M., & Smith, N. 2024, arXiv e-prints, arXiv:2407.16113

Renzo, M., Zapartas, E., Justham, S., et al. 2023, *ApJl*, 942, L32

Romagnolo, A., Belczynski, K., Klencki, J., et al. 2023, *MNRAS*, 525, 706

Romagnolo, A., Gormaz-Matamala, A. C., & Belczynski, K. 2024, *ApJl*, 964, L23

Romagnolo, A., Klencki, J., Vigna-Gómez, A., & Belczynski, K. 2025, *A&A*, 693, A137

Sabahit, G. N., Vink, J. S., Higgins, E. R., & Sander, A. A. C. 2022, *MNRAS*, 514, 3736

Sabahit, G. N., Vink, J. S., Sander, A. A. C., & Higgins, E. R. 2023, *MNRAS*, 524, 1529

Saha, M. N. 1920, *The London, Edinburgh, and Dublin Philosophical Magazine and Journal of Science*, 40, 472

—. 1921, *Proceedings of the Royal Society of London. Series A, Containing Papers of a Mathematical and Physical Character*, 99, 135

Sana, H., de Mink, S. E., de Koter, A., et al. 2012, *Science*, 337, 444

Sander, A. A. C., Hamann, W. R., Todt, H., Hainich, R., & Shenar, T. 2017, *A&A*, 603, A86

Sander, A. A. C., Hamann, W. R., Todt, H., et al. 2019, *A&A*, 621, A92

Sander, A. A. C., Lefever, R. R., Poniatkowski, L. G., et al. 2023, *A&A*, 670, A83

Sander, A. A. C., & Vink, J. S. 2020, *MNRAS*, 499, 873

Sander, A. A. C., Vink, J. S., & Hamann, W. R. 2020, *MNRAS*, 491, 4406

Sander, A. A. C., Lefever, R. R., Josiek, J., et al. 2025, *Discovery of a new transitional type of evolved massive stars with hard ionizing flux*, arXiv:2508.18410

Schneider, F. R. N., Podsiadlowski, P., & Laplace, E. 2024, *A&A*, 686, A45

Shenar, T. 2024, arXiv e-prints, arXiv:2410.04436

Shenar, T., Sablowski, D. P., Hainich, R., et al. 2019, *Astronomy & Astrophysics*

Shenar, T., Sablowski, D. P., Hainich, R., et al. 2020, *A&A*, 641, C2

Smith, N. 2014, *ARAA*, 52, 487

Spruit, H. C. 2002, *A&A*, 381, 923

Tabernero, H. M., Dorda, R., Negueruela, I., & González-Fernández, C. 2018, *MNRAS*, 476, 3106

Taylor, R. J. 1973, *Monthly Notices of the Royal Astronomical Society*, 161, 365

Tehrani, K. A., Crowther, P. A., Bestenlehner, J. M., et al. 2019, *MNRAS*, 484, 2692

Toonen, S., Hamers, A., & Portegies Zwart, S. 2016, *Computational Astrophysics and Cosmology*, 3, 6

Townsend, R. H. D., & Teitler, S. A. 2013, *MNRAS*, 435, 3406

Ugolini, C., Limongi, M., Schneider, R., et al. 2025, *The initial mass-remnant mass relation for core collapse supernovae*, arXiv:2501.18689

van Loon, L., Cioni, M.-R., Zijlstra, A. A., & Loup, C. 2005, *A&A*, 438, 273

Verhamme, O., Sundqvist, J., de Koter, A., et al. 2024, arXiv e-prints, arXiv:2410.14937

Vink, J. S. 2015, *The True origin of Wolf-Rayet stars*, arXiv:1510.00227

—. 2017, *A&A*, 607, L8

Vink, J. S., & de Koter, A. 2005, *A&A*, 442, 587

Vink, J. S., de Koter, A., & Lamers, H. J. G. L. M. 1999, *A&A*, 350, 181

—. 2000, *A&A*, 362, 295

—. 2001, *A&A*, 369, 574

Vink, J. S., & Gräfener, G. 2012, *ApJl*, 751, L34

Vink, J. S., Higgins, E. R., Sander, A. A. C., & Sabahit, G. N. 2021, *MNRAS*, 504, 146

Vink, J. S., Muijres, L. E., Anthonisse, B., et al. 2011, *A&A*, 531, A132

Vink, J. S., & Sander, A. A. C. 2021, *MNRAS*, 504, 2051

Šurlan, B., Hamann, W. R., Aret, A., et al. 2013, *A&A*, 559, A130

Šurlan, B., Hamann, W. R., Kubát, J., Oskinova, L. M., & Feldmeier, A. 2012, *A&A*, 541, A37

Vynayethya, P., Ryu, T., Wang, C., Sills, A., & Pakmor, R. 2025, *The collision and merger products of stars do not look alike: A magnetohydrodynamics comparison*, arXiv:2510.13736

Wang, L., Gies, D. R., & Peters, G. J. 2017, *The Astrophysical Journal*, 843, 60

—. 2018, *The Astrophysical Journal*, 853, 156

Wang, L., Gies, D. R., Peters, G. J., et al. 2021, *The Astronomical Journal*, 161, 248

Wickramasinghe, D. T., Tout, C. A., & Ferrario, L. 2014, *MNRAS*, 437, 675

Yang, M., Bonanos, A. Z., Jiang, B., et al. 2023, *A&A*, 676, A84

Yoon, S.-C., & Cantiello, M. 2010, *ApJl*, 717, L62

Yoon, S. C., Langer, N., & Norman, C. 2006, *A&A*, 460, 199

Yusof, N., Hirschi, R., Meynet, G., et al. 2013, *MNRAS*, 433, 1114

Zapartas, E., de Wit, S., Antoniadis, K., et al. 2025, *A&A*, 697, A167

the reviewing process simpler for authors and referees alike. Learn more at <http://astro.theoj.org>.

This paper was built using the Open Journal of Astrophysics L^AT_EX template. The OJA is a journal which provides fast and easy peer review for new papers in the **astro-ph** section of the arXiv, making